RAA 2017 Vol. **17** No. **6**, 52 (20pp) doi: 10.1088/1674–4527/17/6/52

http://www.raa-journal.org *http://iopscience.iop.org/raa*

***R**esearch in*
***A**stronomy and*
***A**strophysics*

Weak gravitational lensing of quantum perturbed lukewarm black holes and cosmological constant effect

Hossein Ghaffarnejad and Mojtaba Amir Mojahedi

Faculty of Physics, Semnan University, Semnan 35131-19111, Iran;
hghafarnejad@semnan.ac.ir, amirmojahed@semnan.ac.ir

Received 2016 June 29; accepted 2017 February 8

Abstract The aim of the paper is to study weak gravitational lensing of quantum (perturbed) and classical lukewarm black holes (QLBHs and CLBHs respectively) in the presence of cosmological parameter Λ. We apply a numerical method to evaluate the deflection angle of bending light rays, image locations θ of sample source $\beta = -\frac{\pi}{4}$, and corresponding magnifications μ. There are no obtained real values for Einstein ring locations $\theta_E(\beta = 0)$ for CLBHs but we calculate them for QLBHs. As an experimental test of our calculations, we choose mass M of 60 types of the most massive observed galactic black holes acting as a gravitational lens and study quantum matter field effects on the angle of bending light rays in the presence of cosmological constant effects. We calculate locations of non-relativistic images and corresponding magnifications. Numerical diagrams show that the quantum matter effects cause absolute values of the quantum deflection angle to be reduced with respect to the classical ones. The sign of the quantum deflection angle is changed with respect to the classical values in the presence of the cosmological constant. This means dominance of the anti-gravity counterpart of the cosmological horizon on the angle of bending light rays with respect to absorbing effects of 60 local types of the most massive observed black holes. Variations of the image positions and magnifications are negligible when increasing dimensionless cosmological constant $\epsilon = \frac{16\Lambda M^2}{3}$. The deflection angle takes positive (negative) values for CLBHs (QLBHs) and they decrease very fast (slowly) by increasing the closest distance x_0 of bending light ray and/or dimensionless cosmological parameter for sample giant black holes with $0.001 < \epsilon < 0.01$.

Key words: gravitational lensing: weak — strong — micro — stars: black holes

1 INTRODUCTION

Gravitational deflection of light rays is one of the experimental tests of the general theory of relativity. This effect is observed in the presence of interstellar and large scale objects, for instance stars, black holes and clusters of galaxies (Schneider et al. 1992; Petters et al. 2001, see also Schneider 2006 and references therein). Gravitational lensing in weak field limits can be used to measure masses of interstellar objects. Microlensing is observed in cosmic sources called galactic microlensing. In the latter case, there are only elementary and secondary images made. Source and observer are assumed to be located in asymptotically flat regions of the lens. Multiple relativistic images are formed via strong gravitational lensing where the light ray moves very close to a black hole's photon sphere and circulates about the lens (black hole) before it arrives at the observer. In fact, exact analytic solutions of the null geodesics, gravitational lens equations and deflection angle of light for the Kerr-Newman and Kerr-Newman-(anti) de Sitter black holes have been studied and derived for the first time in Kraniotis (2014). The solutions are expressed in terms of generalized hypergeometric functions of Appell-Lauricella and Weierstrass elliptic functions. There, all the parameters of the theory, including mass, spin, electric charge and cosmological constant, enter the solutions on an equal footing (a Reissner-

Nordstrom-de Sitter (RNdS) black hole is a special case of Kerr-Newman-de Sitter (KNdS)). In the absence of a cosmological constant, the influence of electric charge is studied by Eiroa et al. for Reissner-Nordstrom (RN) black hole strong lensing (Eiroa et al. 2002). They obtained its relativistic image. The influence of the cosmological constant is studied on gravitational lensing by Sereno (Sereno 2008) in which the effects of the cosmological constant are negligible near the lens but not at distances far from the lens. At these large distances, the unresolved images are slightly de-magnified, radius of the Einstein ring decreases and time delay increases. Gravitational lensing of a Kerr black hole is studied in the weak field limits (Sereno & de Luca 2006) where the critical curves are still circles displaced from the black hole location in the equatorial direction and the corresponding caustic is point-like. In strong deflection limits, Kerr black hole gravitational lensing is studied in Bozza et al. (2006) in which all observational quantities, namely image locations, magnifications, etc., depend on the projection of the spin on a plane which is orthogonal to the line of sight. Gravitational lensing is also studied from wormholes and naked singularities. For instance, strong deflection limits of a Janis-Newman-Winnicour (JNW) wormhole and Ellis wormhole gravitational lensing are studied in Dey & Sen (2008). The JNW wormhole generates relativistic images, but not the Ellis wormhole due to the absence of its photon sphere. Gravitational lensing from rotating naked singularities is studied (see Gyulchev & Yazadjiev 2008) in the presence of massless scalar fields in which scalar charge has an important effect on the magnification signature (parity of the images) and displacement of critical curves, but not on the point-like caustics.

In other words, the point like caustics are moved away from the optical axis without affecting the scalar charge. Locations of the relativistic images and their separability for weakly naked singularities are computed in the strong deflection limits by using a numerical method. The role of the scalar field is studied in gravitational lensing (Virbhadra et al. 1998) where a spherically symmetric static lens is characterized by its mass and scalar charge parameters. Usually, the nonlinear electromagnetic fields of the black hole charge cause the causal singularity of the black holes to be eliminated. In the latter case, they reach regular supermassive black holes located at the centers of galaxies. The first regular black hole was introduced by Bardeen (Bardeen 1968, Eiroa & Sendra 2011). This is obtained from the Einstein field equation with a nonlinear electromagnetic source (Ayón-Beato & García 2000, Ansoldi 2008).

In this work, we assume that a quantum perturbed lukewarm black hole (QLBH) metric is a gravitational lens. Then we study its gravitational lensing for weak deflection limits of bending light rays. The metric of the QLBH was obtained (Ghaffarnejad et al. 2013) by solving the well known backreaction metric equation where the renormalized expectation value of the stress tensor operator of a massless quantum scalar field is located in the right side of the Einstein equation. It will be the quantum counterpart of the source and causes the RNdS black hole to evaporate when its initial Arnowitt-Deser-Misner (ADM) mass 'M' is equal to its electric charge. In Ghaffarnejad et al. (2013) we showed that its final state reaches a remnant stable mini black hole. All observational quantities, for instance locations of non-relativistic images and magnifications, are studied for a QLBH and compared with results of a classical lukewarm black hole (CLBH) lens. We will use a numerical method to solve the lens equation and calculate the corresponding magnifications. As an experimental test of our numerical calculations, we use 60 types of the most massive observed galactic back holes as the gravitational lenses and study their mass absorbing effect versus the anti-gravity effects of the cosmological constant on the quantum (classical) deflection angle of bending light rays in the presence (absence) of quantum scalar field effects.

The paper is organized as follows. In Section 2 we review CLBH and QLBH metrics from Ghaffarnejad et al. (2013). In Section 3 we use a numerical method to evaluate the deflection angle of the bending light ray and plot its diagram against dimensionless cosmological parameter ϵ. In Section 4 we obtain elementary and secondary image locations. In Section 5 we evaluate magnifications of the non-relativistic images and plot their numerical diagrams. Section 6 provides the conclusions.

2 CLASSICAL AND QUANTUM LUKEWARM BLACK HOLES

Let us start with the metric of the final state of an evaporating QLBH. This metric was obtained previously in Ghaffarnejad et al. (2013) by solving the backreaction equation via the perturbation method as

$$(2M)^{-2}ds^2 \cong -F_{B,C}(x)d\tau^2 + \frac{dx^2}{F_{B,C}(x)} + x^2(d\theta^2 + \sin^2\theta d\varphi^2)\,, \qquad (1)$$

$$F_{B,C}(x) = 1+\frac{1}{4x^2}-\frac{\rho_{B,C}(x)}{x} -\epsilon\frac{\sigma_{B,C}(x)x^2}{4}, \quad (2)$$

where subscripts of B and C denote the black hole and cosmological horizons regions respectively. We use units where $c=G=\hbar=1$ and define dimensionless quantities

$$\tau = \frac{t}{2M}, \quad x=\frac{r}{2M}, \quad q=\frac{Q}{M}=1, \\ \epsilon = \frac{16\Lambda M^2}{3}, \quad (3)$$

in which Q denotes the black hole electric charge parameter. We call ϵ the dimensionless cosmological parameter in what follows. Up to terms of order ϵ^2, the expanded forms of the perturbation series representing backreaction functions $\rho_{B,C}(x)$ and $\sigma_{B,C}(x)$ are obtained by solving the well known backreaction equation

$$G_{\mu\nu}=-8\pi\Big\{T^{\rm EM}_{\mu\nu}+\langle\hat{T}_{\mu\nu}\rangle_{\rm ren}\Big\},$$

where $T^{\rm EM}_{\mu\nu}$ and $\langle\hat{T}_{\mu\nu}\rangle_{\rm ren}$ are classical electromagnetic field stress tensor and renormalized expectation value of quantum massless, charge-less scalar field stress tensor operator respectively such that

$$\rho_B(x) = \rho(x\to x_B)\simeq\Big\{\frac{U_1(x_B)}{(x-x_B)} -\frac{U_2(x_B)}{(x-x_B)^2}\Big\}\exp\Big\{\frac{U_3(x_B)}{x-x_B}\Big\}, \quad (4)$$

$$\rho_C(x) = \rho(x\to x_C)\simeq\Big\{\frac{U_1(x_C)}{(x_C-x)} -\frac{U_2(x_C)}{(x_C-x)^2}\Big\}\exp\Big\{\frac{U_3(x_C)}{x_C-x}\Big\}, \quad (5)$$

$$\sigma_B(x) = \sigma(x\to x_B)\simeq-\frac{4}{3\epsilon}\Big\{\frac{V_1(x_B)}{(x-x_B)} +\frac{V_2(x_B)}{(x-x_B)^2}\Big\}\exp\Big\{\frac{V_3(x_B)}{x-x_B}\Big\}, \quad (6)$$

and

$$\sigma_C(x) = \sigma(x\to x_C)\simeq-\frac{4}{3\epsilon}\Big\{\frac{V_1(x_C)}{(x_C-x)} +\frac{V_2(x_C)}{(x_C-x)^2}\Big\}\exp\Big\{\frac{V_3(x_C)}{x_C-x}\Big\}, \quad (7)$$

where x_B and x_C are the radius of the black hole and the cosmological event horizon respectively given by

$$x_B=\frac{1}{2}+\frac{\sqrt{\epsilon}}{8}, \quad x_C=\frac{2}{\sqrt{\epsilon}}-\frac{1}{2}-\frac{\sqrt{\epsilon}}{8}. \quad (8)$$

Definitions of the constants $U_{1,2,3}(x_{B,C})$ and $V_{1,2,3}(x_{B,C})$ are provided in Appendix A. The CLBH metric is obtained by solving $G_{\mu\nu}=-8\pi T^{\rm EM}_{\mu\nu}$ (in absence of backreaction corrections of Hawking radiation for quantum massless scalar fields) such that $\rho_{B,C}(x)=1$ and $\sigma_{B,C}(x)=1$. Now, we use the numerical method to calculate the deflection angle of bending light rays for both the QLBH and CLBH metrics as follows.

3 LIGHT DEFLECTION ANGLE

When a light ray moves in the neighborhood of the black hole metric Equation (1) (the quantum lens), it deflects with angle (Weinberg 1972)

$$\alpha=2\int_{x_0\geq x_{\rm ps}}^{x_C(\epsilon)}\frac{1}{x^2}\frac{dx}{\sqrt{1/\tilde{b}^2-F_{B,C}(x,\varepsilon)/x^2}}-\pi\,, \quad (9)$$

where $x_{\rm ps}$ is the photon sphere radius and x_B and x_C are called radiuses of the black hole and the cosmological horizons respectively, given by Equation (8). Here dimensionless impact parameter $\tilde{b}=\frac{b}{2M}$ is written as

$$\tilde{b}=\frac{b}{2M}=\frac{x_0}{\sqrt{F_{B,C}(x_0,\varepsilon)}} \quad (10)$$

in which impact parameter b is defined in terms of constant angular momentum L and energy E of the light ray as $b=|\frac{L}{E}|$. It is coordinate independent and so is invariant of the system, as are the black hole mass M and electric charge Q. The photon sphere radius $x_{\rm ps}$ is obtained by the largest positive root of the equation

$$\frac{d}{dx}\Big(\frac{x^2}{F_B(x)}\Big)\Big|_{x=x_{\rm ps}}\approx 0\,, \quad (11)$$

where an explicit form of the function $F_B(x,\epsilon)$ is obtained by inserting Equation (4) and Equation (6) into Equation (2). The photon sphere defined by Equation (11) is obtained by solving the geodesic equation for a photon moving circularly around the black hole center. The explicit form of the function $F_C(x,\epsilon)$ in Equation (10) is obtained by inserting Equation (7) and Equation (9) into Equation (2). x_0 given in the integration of Equation (9) is the closest approach distance for which the bending light ray reaches the center of the lens. In weak deflection limits of the gravitational lensing, we must restrict the integration of Equation (9) to $x_0>x_{\rm ps}$ for which $|\alpha|<\frac{3\pi}{2}\simeq 4.7$ (radian) and so we still do not have relativistic images. Relativistic images are formed usually via circulation of bending light

rays around the lens center for which deflection angle becomes $|\alpha| > \frac{3\pi}{2}$ (see fig. 1 in Eiroa 2005). For a large galactic black hole we can approximate $\epsilon \simeq 10^{-22}$ experimentally (see Ghaffarnejad et al. 2013) for which Equation (8) reads

$$x_B \approx 0.5, \quad x_C \approx 10^{11}. \tag{12}$$

What should we choose for a particular value of x_0 if we use the sample Equation (12)? To do so we define boundary point $x_{\rm b}$ via

$$F_B(x_{\rm b}, \epsilon) = F_C(x_{\rm b}, \epsilon) \tag{13}$$

and

$$\frac{d}{dx}F_B(x_{\rm b}, \epsilon) = \frac{d}{dx}F_C(x_{\rm b}, \epsilon). \tag{14}$$

The above equations do not give us an analytic solution for $x_{\rm b}$ against ϵ and so we must obtain all possible values by plotting their diagrams. Diagrams of Equations (11) and (2) are plotted against ϵ in the left panel of Figure 1 where the solid line represents $x_{\rm ps}(\epsilon)$ and the dotted line represents $x_{\rm b}(\epsilon)$.

The right panel of Figure 1 features a plot of Equation (14). These two diagrams show that

$$x_{\rm ps} \approx x_{\rm b} < 0.6, \epsilon < 1 \tag{15}$$

and so the functions in Equation (4) and Equation (6) are negligible when we calculate Equation (9) by choosing the following boundary conditions.

$$0.6 \leq x_0 \leq 1.5, \quad x_C \approx 10^{11}; \quad \epsilon = 10^{-22} \tag{16}$$

and/or

$$x_0 = 1.5, x_C = \frac{2}{\sqrt{\epsilon}} - \frac{1}{2} - \frac{\sqrt{\epsilon}}{8}; 0 < \epsilon < 1. \tag{17}$$

We should point out that the dimensionless cosmological parameter given in Equation (16) corresponds to the most massive black holes in the central part of giant galaxies and certainly not for the Milky Way. Inserting Equation (2), Equation (5) and Equation (7), we obtain

$$F_C(x) = 1 + \frac{1}{4x^2} - \frac{\rho_C(x)}{x} - \frac{\epsilon\sigma_C(x)x^2}{4},$$

and we plot the diagram of quantum and classical deflection angles $\alpha_{\rm q}$ and $\alpha_{\rm c}$ respectively defined by Equation (9) against x_0 (ϵ) in the upper-left (right) panel of Figure 2 for a sample of theoretical giant black holes with $0.001 < \epsilon < 0.01$.

The lower-left panel in Figure 2 displays a numerical diagram of the classical and quantum deflection angles of bending light rays for 60 types of experimentally observed most massive galactic black holes lenses. We see that the weak deflection limit satisfies $|\alpha| < \frac{3\pi}{2} \simeq 4.7$ in Figure 2. Quantum deflection angle $\alpha_{\rm q}$ is shown in this figure with $square$ symbols but the classical deflection angle $\alpha_{\rm c}$ is shown with $+$ and/or $\times$ symbols. The lower-right panel in Figure 2 exhibits a schematic diagram of the gravitational lensing setup. The classical deflection angle is evaluated by inserting

$$F(x) = 1 + \frac{1}{4x^2} - \frac{1}{x} - \frac{\epsilon x^2}{4}$$

into Equation (9) and integrating numerically with boundary conditions Equation (16) and/or Equation (17) corresponding to 60 types of observed most massive black hole lenses and theoretical regime $0.001 < \epsilon < 0.01$. We see in the upper-left panel of Figure 2 that the deflection angle decreases by increasing x_0 for CLBHs but not for QLBHs.

In the upper-left panel of Figure 2, we see that relativistic images for CLBH are formed with $\alpha_{\rm c} \to \infty$ and $x_0 \to 1$ but not in the case of QLBHs. We see in the upper-right panel of Figure 2 that the deflection angle decreases faster (slower) for CLBH (QLBHs) by increasing the cosmological parameter ϵ. Also, these diagrams show that the quantum deflection angle sign is changed with respect to the classical one in the presence of the quantum matter field effects. In addition, the absolute value of the quantum deflection angle becomes smaller with respect to the classical one in the presence of quantum matter field effects. Physical effects of quantum field backreaction on the evaporating QLBH event horizon cause its horizon to shrink (Ghaffarnejad et al. 2013) so that its final state reaches a remnant stable mini black hole. In the latter case, the distance of the closest approach of bending light rays becomes larger than what is formed in the classically unperturbed black hole. On the other hand, the conditions given by Equation (13) and Equation (14) tell us that for regions where $x > x_{\rm b} \approx x_{\rm ps}$ we can replace the cosmological counterpart of the backreaction function Equation (5) and Equation (7) to calculate α_q where cosmological anti-gravity (un-absorbing) effects of the background metric F_C dominate the gravitational lensing with respect to absorbing effects of local black hole counterpart F_B. This is a stronger effect in the case of QLBHs because of the reduction of the shrunken horizon in the remnant stable mini quantum black hole. This can be seen in diagrams of classical and quantum deflection angles $\alpha_{c,q}$ given in Figure 2. The QLBH diagram

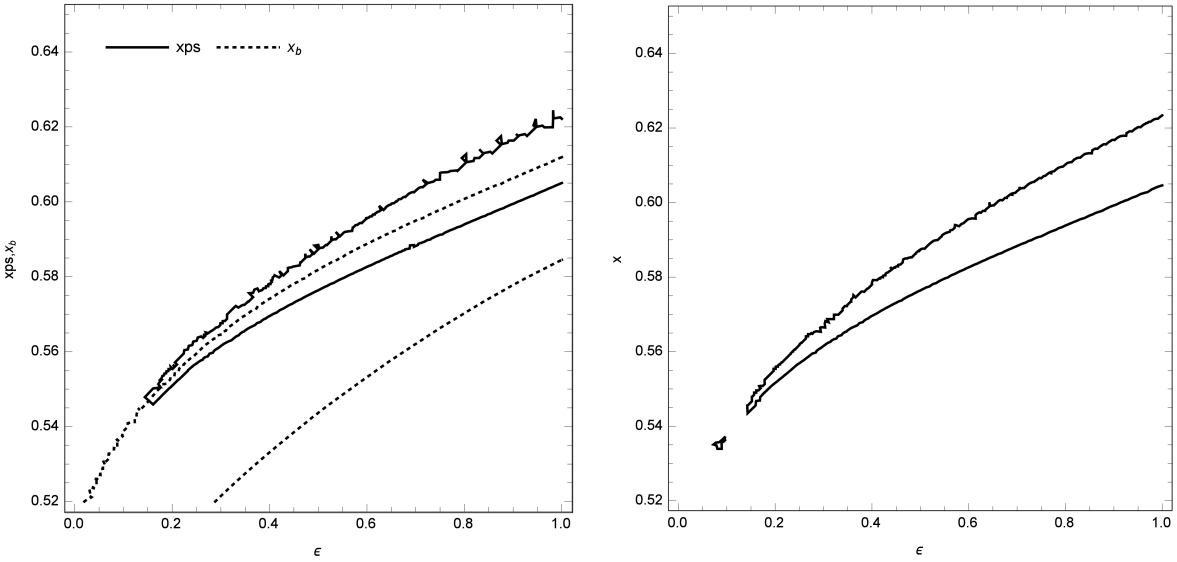

Fig. 1 Left panel shows a diagram of Eqs. (11) and (2) plotted against ϵ with solid and dotted lines respectively. Right panel features a plot of Eq. (14) against ϵ.

has not dramatically changed by raising ϵ and/or $x_{\rm ps}$. But for CLBH, it decreases because of the dominance of the absorbing property of black hole mass with respect to the homogenous acceleration and expanding anti-gravity property of the cosmological constant ϵ and/or absence of quantum matter backreaction corrections. In the next section, we use the above results and seek locations of non-relativistic images.

4 NON-RELATIVISTIC IMAGE LOCATIONS

Several types of gravitational lensing equations (see for instance Bozza 2008; Keeton & Petters 2005) have been proposed, but we choose

$$\tan\beta=\tan\theta-\frac{D_{ds}}{D_s}\Big[\tan\theta+\tan(\alpha-\theta)\Big],\quad(18)$$

where source angular location β is made by crossing observer-lens line and observer-source line (see lower-right panel in Fig. 2). Image location θ is made by crossing observer-lens line and observer-image line. D_{ds} denotes the distance between lens and source. D_s describes the distance between observer and source. We set $\frac{D_{ds}}{D_s}=\frac{1}{2}$ for simplification of the problem.

Applying the numerical method we solve Equation (18) and plot its diagram against ϵ for $\beta=0$ (Einstein rings) and sample source $\beta=-\frac{\pi}{4}$ for QLBH. In the case of CLBH, we do not obtain real values for the location of Einstein rings $\theta_E(\beta=0)$. A diagram of QLBH Einstein rings is given in the right panel of Figure 3 where numerical values ϵ are chosen from the mass of 60 types of observed most massive black holes (see Table 1) which are on the order of $\epsilon\approx 10^{-22}$ satisfying the condition defined by Equation (16) and/or Equation (17). We plot numerical diagrams of non-relativistic image locations for a sample source $\beta=-\frac{\pi}{4}$ from 60 types of experimentally observed most massive galactic black hole lenses in the lower-left (right) panel of Figure 4 for CLBHs (QLBHs). For the theoretical sample, CLBH (QLBH) lens with $0.001<\epsilon<0.01$, diagrams of image locations of the source, $\beta=-\frac{\pi}{4}$ is given in the upper-left (right) panel of Figure 4. All diagrams show that the anti-gravity effects of the dimensionless cosmological constant ϵ are dominant with respect to the local absorbing property of the supermassive black holes because all diagrams treat $\theta(\epsilon)$ as a constant function versus ϵ.

5 MAGNIFICATION

Applying Liouville's theorem, the gravitational lensing causes the surface brightness to be preserved, but it does change the apparent solid angle of a source. This change is evaluated via magnification μ. The amount of magnification is given by the ratio of the image area to the source area and so it is a dimensionless numerical quan-

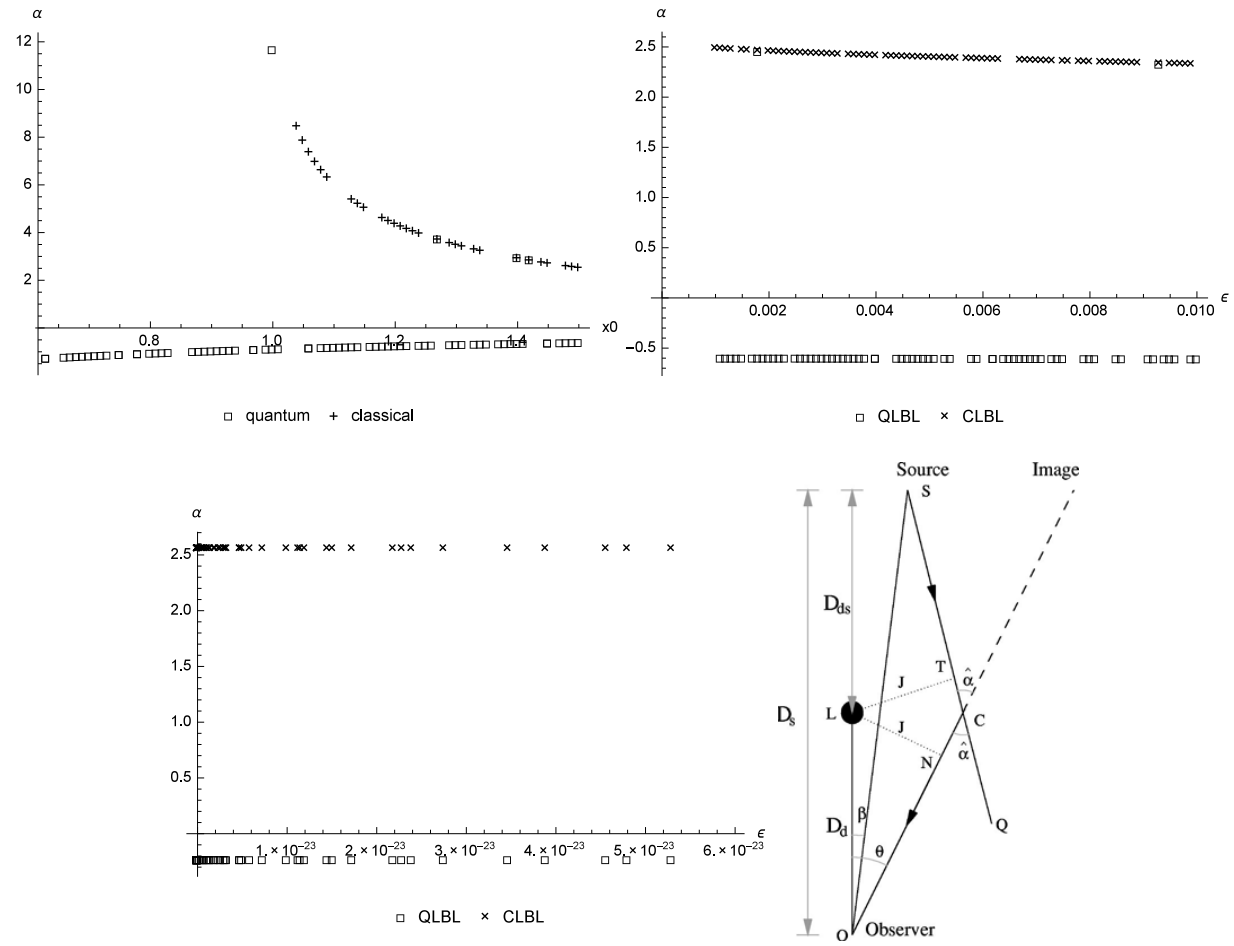

Fig. 2 A diagram of the deflection angle Eq. (9) is plotted against x_0 for $\varepsilon = 10^{-22}, 0.6 < x_0 < 1.5$ (*upper-left panel*) and against ϵ for $x_0 = 1.5, 0.001 < \epsilon < 0.01$ (*upper-right panel*). Diagram of the bending angle α is plotted for the CLBH and QLBH with + and $square$ symbols respectively. *Lower-left panel* displays a diagram of α plotted against ϵ for 60 types of experimentally observed large black holes. *Lower-right panel* demonstrates the gravitational lensing setup.

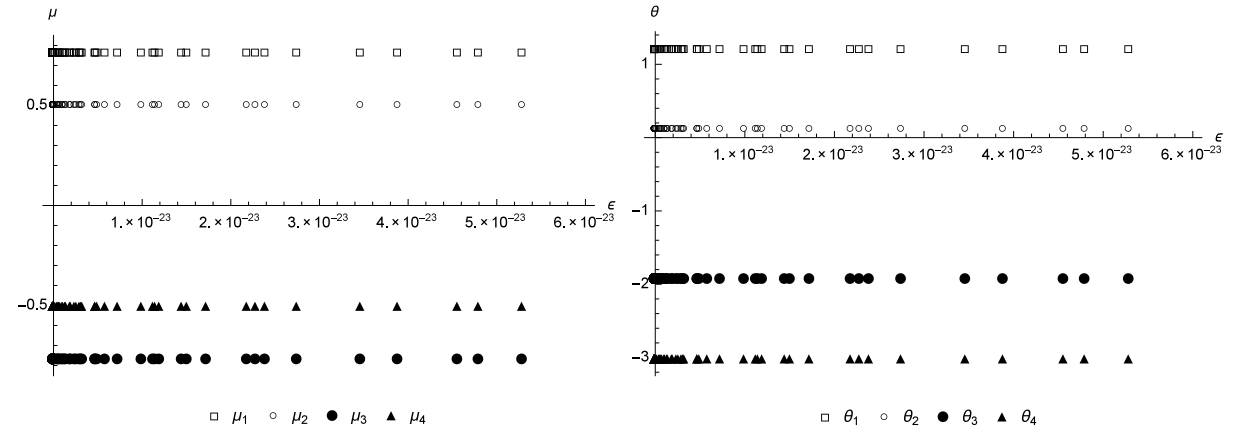

Fig. 3 Angular locations $\theta_{1,2,3,4}$ and corresponding magnifications $\mu_{1,2,3,4}$ of Einstein rings $(\beta = 0)$ for QLBH. We have not obtained real values for CLBH.

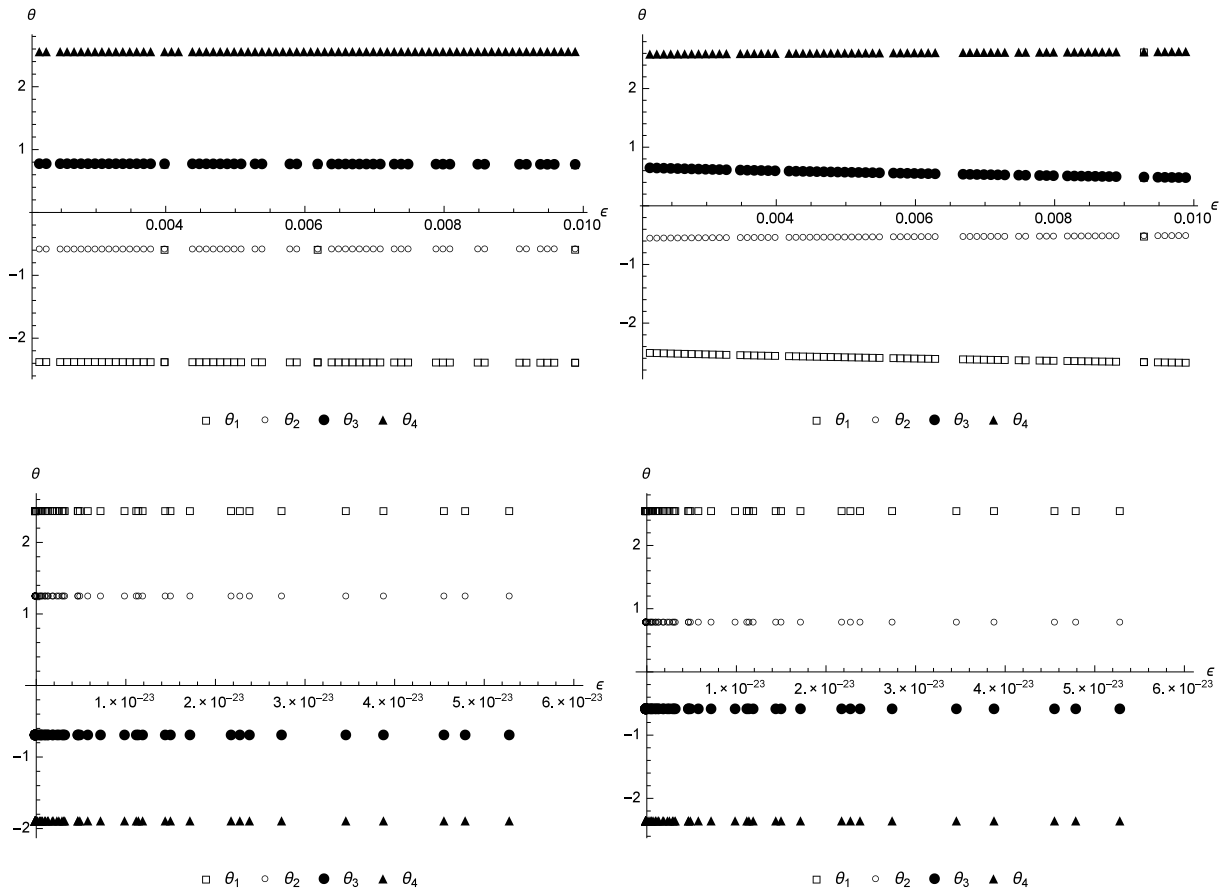

Fig. 4 Upper panels are image angular locations $\theta_{1,2,3,4}$ of sample source $\beta = -\frac{\pi}{4}$ plotted against ϵ for QLBH (*left panel*) and CLBH (*right panel*). Lower panels are image angular locations for 60 kinds of observed large black holes which represent QLBH (*left*) and CLBH (*right*) types.

tity. Usually, it is found to be larger than one in size but when its amount becomes less than one then it refers to a reduction in size, which is sometimes called "demagnification." The magnification formula is given by

$$\mu = \mu_{\rm t}\mu_{\rm r} = \left(\frac{\sin\theta}{\sin\beta}\right)\left(\frac{d\theta}{d\beta}\right), \tag{19}$$

where $\mu_{\rm t}$ and $\mu_{\rm r}$ defined by

$$\mu_{\rm t} = \frac{\sin\theta}{\sin\beta}, \quad \mu_{\rm r} = \frac{d\theta}{d\beta} \tag{20}$$

are called tangential and radial magnifications respectively. Eliminating β via Equation (18) and assuming $\frac{D_{d,s}}{D_s} = \frac{1}{2}$, Equations (19) and (2) become respectively

$$\mu^{\pm}(\theta) = \frac{\pm 2\csc\left\{\tan^{-1}\left[\frac{1}{2}(\tan(\theta-\alpha)+\tan\theta)\right]\right\}}{\sec^2(\alpha-\theta)+\sec^2\theta} \times \sec^2\left\{\tan^{-1}\left[\frac{1}{2}(\tan(\theta-\alpha)+\tan\theta)\right]\right\}\sin\theta, \tag{21}$$

and

$$\mu_{\rm r}(\theta) = \frac{2\sec^2\left\{\tan^{-1}\left[\frac{1}{2}(\tan(\theta-\alpha)+\tan\theta)\right]\right\}}{\sec^2(\alpha-\theta)+\sec^2\theta}, \tag{22}$$

$$\mu_{\rm t}^{\pm}(\theta) = \pm\csc\left\{\tan^{-1}\left[\frac{1}{2}(\tan(\theta-\alpha)+\tan\theta)\right]\right\} \times\sin\theta. \tag{23}$$

In the case of CLBH, we do not obtain real values for the locations of Einstein rings $\theta_E(\beta = 0)$ and so their magnifications will not have real values. Diagrams illustrating magnifications of QLBH Einstein rings are given in the left panel of Figure 3 where numerical values ϵ are chosen from the mass of 60 types of observed most massive black holes, which are on the order of $\epsilon \approx 10^{-22}$.

In Figure 5, we plot numerical diagrams of non-relativistic image magnifications of a sample source $\beta =$

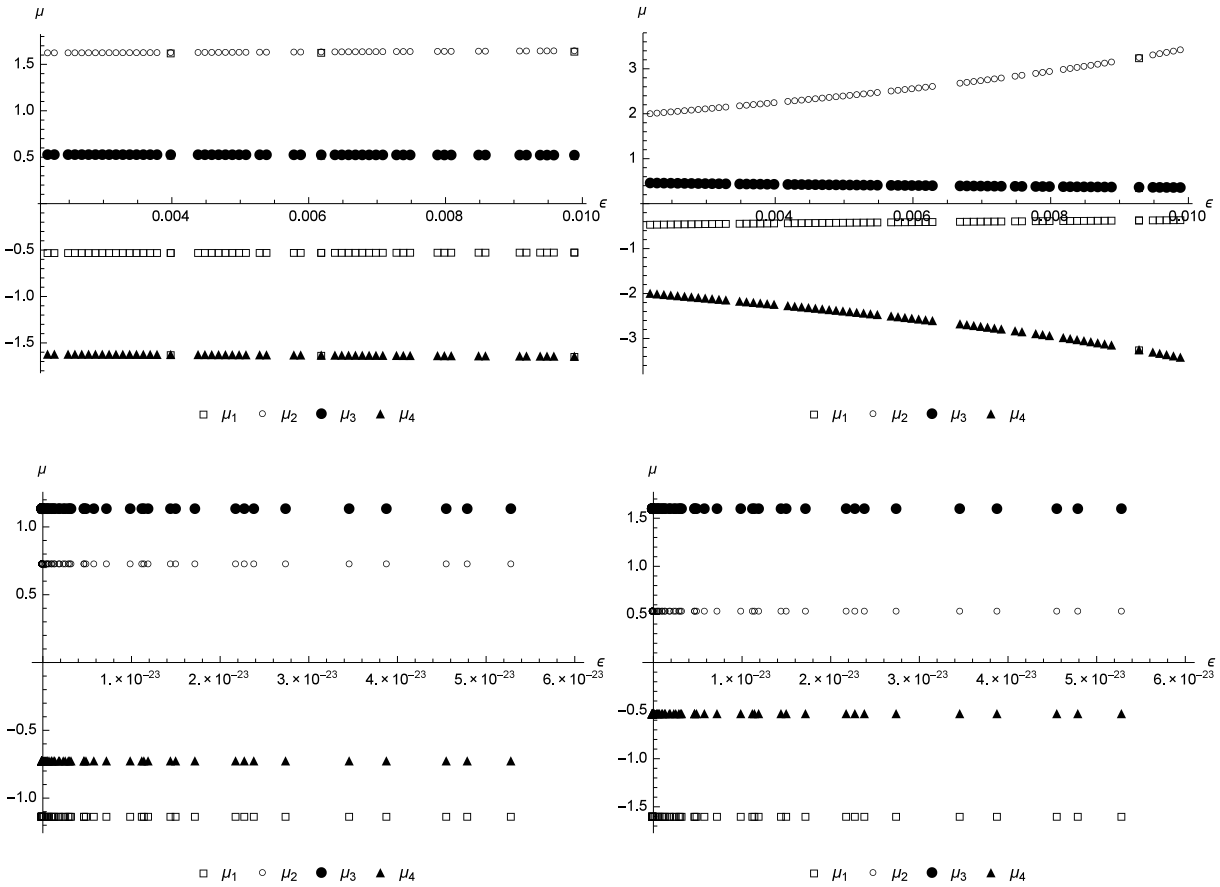

Fig. 5 Upper panels illustrate magnification of image positions $\theta_{1,2,3,4}$ of sample source $\beta = -\frac{\pi}{4}$ plotted against ϵ for QLBH (*left panel*) and CLBH (*right panel*). Lower left (right)-panel shows a diagram of magnification $\mu_{1,2,3,4}$ of non-relativistic images plotted against ϵ for 60 kinds of experimentally observed QLBH (CLBH) large black holes.

$-\frac{\pi}{4}$ from 60 types of experimentally observed most massive galactic black holes with $\epsilon \approx 10^{-22}$ and for the theoretical sample with $0.001 < \epsilon < 0.01$. Diagrams show magnifications rise by increasing dimensionless cosmological constant ϵ for regime $0.001 < \epsilon < 0.01$ (see upper-right panel in Fig. 5) but show (approximately) constant magnification for observable regime $\epsilon \approx 10^{-12}$ (see lower-right panel in Fig. 5).

As a future work, we would like to consider gravitational lensing of a quantum perturbed rotating black hole background which is a more realistic background. Casals et al. (2016) studied quantum fields on a rotating Banados-Teitelboim-Zanelli (BTZ) black hole and recently obtained a quantum perturbed metric in analytic form. For given values of black hole mass and angular momentum, they found that the quantum effects lead to a growth in both the event horizon and the radius of the ergosphere, reducing the angular momentum compared to unperturbed values. Also, quantum effects give rise to the formation of a curvature singularity at the Cauchy horizon but show no evidence of super-radiant instability. The BTZ black hole metric solution was obtained in 1992 (Banados et al. 1992), where it came as a surprise because it was believed that no black hole solutions can exist for a negative cosmological constant. The BTZ black hole, which is 3-dimensional, has remarkably similar properties to the 3+1 dimensional black hole, which would exist in our real universe. When the cosmological constant is zero, a vacuum solution of (2+1)-dimensional gravity is necessarily flat (the Weyl tensor vanishes in three dimensions, while the Ricci tensor vanishes due to the Einstein field equations, so the full Riemann tensor vanishes), and it can be shown that no black hole solutions with event horizons exist. By introducing dilatons, we can have black holes. We do have conical angle deficit solutions, but they do not have event horizons. It therefore came as a surprise when black hole solutions were shown to exist for a negative cosmological constant. The

BTZ 3-dimensional black hole has properties similar to ordinary black holes in 3+1 dimensions as follows: (a) It satisfies the 'no hair theorem.' (b) It has the same thermodynamical properties, namely its entropy is captured by a law directly analogous to the Bekenstein bound in (3+1)-dimensions, essentially with the surface area replaced by the BTZ black hole's circumference. (c) Like the Kerr black hole, a rotating BTZ black hole contains an inner and an outer event horizon together with an ergosphere. The BTZ black hole could arise from collapsing matter and its energy-momentum tensor is calculated the same as (3+1) black holes in Carlip (1995). In short, BTZ black holes without any electric charge are locally isometric to anti-de Sitter space.

However, we should use our quantum framework to obtain physical effects of angular momentum associated with the Kerr and/or the BTZ rotating black holes on the gravitational lensing of light rays which can be chosen as the next challenge in this subject. At least as far as we can tell, some physical interpretation about the effect of angular momentum associated with the black hole lens on the gravitational lensing is as follows: All rotating black holes have an ergosphere region which is treated as a particle accelerator. Ejecting particles from the ergosphere to regions far from the black hole photon sphere region affects moving photons and so deviates their velocity and direction, which they do in the post Newtonian limits because of rotating black holes' Coriolis acceleration. These finally affect image locations and their magnifications.

Now we list 60 types of observed supermassive galactic black holes to obtain quantum characteristics for gravitational lensing given in Tables 2–4 as follows.

6 CONCLUSIONS

In this paper, we studied weak gravitational lensing of QLBL and CLBL in the presence of the dimensionless cosmological constant parameter ϵ. In weak deflection limits, we obtained diagrams of deflection angle integral, non-relativistic image locations and corresponding magnifications against ϵ numerically. For experimental results of our work, we choose 60 types of the most massive observed black hole mass to be the experimental gravitational lens and obtained the deflection angle of bending light rays, and their non-relativistic image locations and magnifications in both the CLBH and QLBH regimes. Our work predicts the dominance of the anti-gravity property of the cosmological constant effect versus the mass absorbing effects of most massive galactic black holes on the weak gravitational lensing of the bending light rays. The sign of the quantum deflection angle is changed with respect to the classical deflection angle. The absolute value of the quantum deflection angle reduces with respect to the classical deflection angle of bending light rays for all values of dimensionless cosmological constant. As future work, we will proceed to study our quantum framework that can be applied to the most massive rotating galactic black holes, including Kerr and/or BTZ cases, which have more realistic backgrounds. Ejecting particles from their ergosphere interferes with photons moving around the black hole photon sphere and so causes their velocity and direction to deviate.

Appendix A:

The constants $U_{1,2,3}(x_{B,C})$ and $V_{1,2,3}(x_{B,C})$ are calculated in Ghaffarnejad et al. (2013) as follows:

$$U_1(x_B) = \frac{\pi}{12} + \frac{4x_B^4[A(x_B)+B(x_B)/6]}{3} - \frac{16\pi M^2 C_2 x_B^4}{3}, \tag{A.1}$$

$$U_2(x_B) = \frac{2\pi x_B^5[A(x_B)-8\pi M^2 C_2]}{3G(x_B)}, \tag{A.2}$$

$$U_3(x_B) = 2x_B^3[A(x_B)-8\pi M^2 C_2]. \tag{A.3}$$

$$U_1(x_C) = \pi/24 + 2x_C^4[A(x_C)+B(x_C)/6]/3 - 8\pi M^2 C_2 x_C^4/3, \tag{A.4}$$

$$U_2(x_C) = \frac{\pi x_C^3(1+4x_C^2)}{2G(x_C)}\Big[\frac{\pi}{4} + 4A(x_C) + \frac{2B(x_C)}{3} - 16\pi M^2 C_2\Big][A(x_C) - 8\pi M^2 C_2], \tag{A.5}$$

$$U_3(x_C) = -\frac{x_C^3[A(x_C)-8\pi M^2 C_2]}{2}. \tag{A.6}$$

$$V_1(x_B) = \pi/3x_B^3 + 4x_B[A(x_B)+B(x_B)/6] - 16\pi M^2 x_B C_2, \tag{A.7}$$

$$V_2(x_B) = \frac{2\pi x_B^2[A(x_B)-8\pi M^2 C_2]}{G(x_B)}, \tag{A.8}$$

Table 1 List of Observed Supermassive Black Holes, $M_{\odot} \sim 1.99\times10^{30}$ kg

No.	Name	Mass ($M/M_{\odot}$)	Reference
1	S5 0014+81	4×10^{10}	Ghisellini et al. (2009, 2010),Gaensler (2012)
2	SDSS J102325.31+514251.0	3.31×10^{10}	Zuo et al. (2015)
3	Black hole of central quasar of H1821+643	3×10^{10}	Walker et al. (2014)
4	APM 08279+5255	2.3×10^{10}	Lewis et al. (1998)
5	NGC 4889	2.1×10^{10}	McConnell et al. (2011)
6	Black hole of central elliptical galaxy of Phoenix Cluster	2.0×10^{10}	McDonald et al. (2012)
7	SDSS J074521.78+734336	1.95×10^{10}	Zuo et al. (2015)
8	OJ 287 primary	1.8×10^{10}	Valtonen et al. (2012)
9	NGC 1600	1.7×10^{10}	NASA: 2016[1]
10	SDSS J08019.69+373047.3	1.514×10^{10}	Zuo et al. (2015)
11	SDSS J115954.33+201921.1	1.412×10^{10}	Zuo et al. (2015)
12	SDSS J075303.34+423130.8	1.38×10^{10}	Zuo et al. (2015)
13	SDSS J080430.56+542041.1	1.35×10^{10}	Zuo et al. (2015)
14	SDSS J081855.77+095848.0	1.2×10^{10}	Zuo et al. (2015)
15	SDSS J0100+2802	1.2×10^{10}	Wu et al. (2015)[2]
16	SDSS J082535.19+512706.3	1.122×10^{10}	Zuo et al. (2015)
17	SDSS J013127.34-032100.1	1.1×10^{10}	Ghisellini et al. (2015)
18	Black hole of central elliptical galaxy of MS 0735.6+7421	1.0×10^{10}	NASA/Marshal 2005[3]
19	PSO J334.2028+01.4075	1.0×10^{10}	Liu et al. (2015)
20	Black hole of central elliptical galaxy of RX J1532.9+3021	1.0×10^{10}	Hlavacek-Larrondo et al. (2013)
21	QSO B2126-158	1.0×10^{10}	Ghisellini et al. (2010)
22	Holmberg 15A	1.0×10^{10}	López-Cruz et al. (2014)
23	SDSS J015741.57-010629.6	9.8×10^{9}	Zuo et al. (2015)
24	NGC 3842, Brightest galaxy in the Leo Cluster	9.7×10^{9}	McConnell et al. (2011)
25	SDSS J230301.45-093930.7	9.12×10^{9}	Zuo et al. (2015)
26	SDSS J075819.70+202300.9	7.8×10^{9}	Zuo et al. (2015)
27	CID-947	7.0×10^{9}	Trakhtenbrot et al. (2015)
28	SDSS J080956.02+502000.9	6.45×10^{9}	Zuo et al. (2015)
29	SDSS J014214.75+002324.2	6.31×10^{9}	Zuo et al. (2015)
30	Messier 87	6.30×10^{9}	Walsh et al. (2013)
31	SDSS J025905.63+001121.9	5.25×10^{9}	Zuo et al. (2015)
32	SDSS J094202.04+042244.5	5.13×10^{9}	Zuo et al. (2015)
33	QSO B0746+254	5.0×10^{9}	Ghisellini et al. (2010)
34	QSO B2149-306	5.0×10^{9}	Ghisellini et al. (2010)
35	NGC 1277	5.0×10^{9}	Emsellem (2013)
36	SDSS J090033.50+421547.0	4.7×10^{9}	Zuo et al. (2015)
37	Messier 60	4.5×10^{9}	Shen & Gebhardt (2010)
38	SDSS J011521.20+152453.3	4.1×10^{9}	Zuo et al. (2015)
39	QSO B0222+185	4.0×10^{9}	Ghisellini et al. (2010)
40	Hercules A (3C 348)	4.0×10^{9}	Alberto et al. (2002)
41	SDSS J213023.61+122252.0	3.5×10^{9}	Zuo et al. (2015)
42	SDSS J173352.23+540030.4	3.4×10^{9}	Zuo et al. (2015)
43	SDSS J025021.76-075749.9	3.1×10^{9}	Zuo et al. (2015)
44	SDSS J030341.04-002321.9	3.0×10^{9}	Zuo et al. (2015)
45	QSO B0836+710	3.0×10^{9}	Ghisellini et al. (2010)
46	SDSS J224956.08+000218.0	2.63×10^{9}	Zuo et al. (2015)
47	SDSS J030449.85-000813.4	2.4×10^{9}	Zuo et al. (2015)
48	SDSS J234625.66-001600.4	2.24×10^{9}	Zuo et al. (2015)
49	ULAS J1120+0641	2.0×10^{9}	Mortlock et al. (2011), Matson (2011)
50	QSO 0537-286	2.0×10^{9}	Ghisellini et al. (2010)
51	NGC 3115	2.0×10^{9}	Kormendy & Richstone (1992)
52	Q0906+6930	2.0×10^{9}	Romani (2006)
53	QSO B0805+614	1.5×10^{9}	Ghisellini et al. (2010)
54	Messier 84	1.5×10^{9}	Bower et al. (1998)
55	QSO B225155+2217	1.0×10^{9}	Ghisellini et al. (2010)
56	QSO B1210+330	1.0×10^{9}	Ghisellini et al. (2010)
57	NGC 6166, Central galaxy of Abell 2199	1.0×10^{9}	Bender et al. (2015)
58	Cygnus A	1.0×10^{9}	Hubble Site 2015[4]
59	Sombrero Galaxy	1.0×10^{9}	Kormendy et al. (1996)
60	Messier 49	1.0×10^{9}	Loewenstein et al. (2001)

Notes: [1] *http://www.nasa.gov/feature/goddard/2016/behemoth-black-hole-found-in-an-unlikely-place*; [2] *Sci-News.com*, Astronomers Discover Record-Breaking Quasar; [3] Most Powerful Eruption In The Universe Discovered NASA/Marshall Space Flight Center (ScienceDaily) January 6, 2005; [4] Black Holes: Gravity's Relentless Pull interactive: Encyclopedia.

Table 2 Quantum Lensing Characteristics for Observed Most Massive Black Holes 1 to 60, $\mu_4 = -\mu_2, \mu_3 = -\mu_1$

Characteristics	1	2	3	4	5
ϵ	1.9×10^{-22}	1.3×10^{-22}	1.1×10^{-22}	6.3×10^{-23}	5.3×10^{-23}
$x_{\rm b}$	0.5	0.5	0.5	0.5	0.5
$x_{\rm c}$	1.4×10^{11}	1.7×10^{11}	1.9×10^{11}	2.5×10^{11}	2.7×10^{11}
$A(x_{\rm b})$	-8.9×10^{-16}	-4.4×10^{-16}	-8.9×10^{-16}	-4.4×10^{-16}	-4.4×10^{-16}
$A(x_{\rm c})$	2.2×10^{-34}	1.3×10^{-34}	9.4×10^{-35}	4.2×10^{-35}	3.2×10^{-35}
$B(x_{\rm b})$	-9.6×10^{-23}	-6.6×10^{-23}	-5.4×10^{-23}	-3.2×10^{-23}	-2.6×10^{-23}
$B(x_{\rm c})$	-2.5×10^{-38}	$-1. \times 10^{-38}$	-1.3×10^{-38}	$-7. \times 10^{-39}$	3.4×10^{-39}
$U_1(x_{\rm c})$	2.3×10^{29}	2.5×10^{29}	7.3×10^{29}	1.1×10^{30}	1.5×10^{30}
$U_2(x_{\rm c})$	1.9×10^{33}	3.3×10^{33}	4.4×10^{33}	9.8×10^{33}	1.3×10^{34}
$U_3(x_{\rm c})$	-2.4×10^{18}	-2.1×10^{18}	-5.7×10^{18}	-6.3×10^{18}	-8.3×10^{18}
$U_1(x_{\rm b})$	0.26	0.26	0.26	0.26	0.26
$U_2(x_{\rm b})$	1.5×10^{-17}	7.4×10^{-18}	1.5×10^{-17}	7.4×10^{-18}	7.4×10^{-18}
$U_3(x_{\rm b})$	1.8×10^{-16}	8.9×10^{-17}	1.8×10^{-16}	8.9×10^{-17}	8.9×10^{-17}
$V_1(x_{\rm c})$	0.00023	0.00014	0.00031	0.0002	0.00022
$V_2(x_{\rm c})$	5.2×10^{7}	3.8×10^{7}	9.3×10^{7}	7.9×10^{7}	9.5×10^{7}
$V_3(x_{\rm c})$	-2.4×10^{18}	-2.1×10^{18}	-5.7×10^{18}	-6.3×10^{18}	-8.3×10^{18}
$V_1(x_{\rm b})$	8.4	8.4	8.4	8.4	8.4
$V_2(x_{\rm b})$	3.6×10^{-16}	1.8×10^{-16}	3.6×10^{-16}	1.8×10^{-16}	1.8×10^{-16}
$V_3(x_{\rm b})$	1.8×10^{-16}	8.9×10^{-17}	1.8×10^{-16}	8.9×10^{-17}	8.9×10^{-17}
$\alpha_{\rm c}$	2.553	2.553	2.553	2.553	2.553
θ_1^c	-2.357	-2.357	-2.357	-2.357	-2.357
θ_2^c	-0.5877	-0.5877	-0.5877	-0.5877	-0.5877
θ_3^c	0.7842	0.7842	0.7842	0.7842	0.7842
θ_4^c	2.554	2.554	2.554	2.554	2.554
μ_1^c	-0.5318	-0.5318	-0.5318	-0.5318	-0.5318
μ_2^c	1.597	1.597	1.597	1.597	1.597
μ_3^c	0.5318	0.5318	0.5318	0.5318	0.5318
μ_4^c	-1.597	-1.597	-1.597	-1.597	-1.597
$\alpha_{\rm q}$	-0.23	-0.23	-0.23	-0.23	-0.23
θ_1^q	-1.9	-1.9	-1.9	-1.9	-1.9
θ_2^q	-0.69	-0.69	-0.69	-0.69	-0.69
θ_3^q	1.2	1.2	1.2	1.2	1.2
θ_4^q	2.4	2.4	2.4	2.4	2.4
μ_1^q	-0.73	-0.73	-0.73	-0.73	-0.73
μ_2^q	1.1	1.1	1.1	1.1	1.1
Characteristics	6	7	8	9	10
ϵ	4.8×10^{-23}	4.6×10^{-23}	3.9×10^{-23}	3.5×10^{-23}	2.8×10^{-23}
$x_{\rm b}$	0.5	0.5	0.5	0.5	0.5
$x_{\rm c}$	2.9×10^{11}	$3. \times 10^{11}$	3.2×10^{11}	3.4×10^{11}	3.8×10^{11}
$A(x_{\rm b})$	-4.4×10^{-16}	-8.9×10^{-16}	-4.4×10^{-16}	-4.4×10^{-16}	-8.9×10^{-16}
$A(x_{\rm c})$	2.8×10^{-35}	2.6×10^{-35}	$2. \times 10^{-35}$	1.7×10^{-35}	1.2×10^{-35}
$B(x_{\rm b})$	-2.4×10^{-23}	-2.3×10^{-23}	-1.9×10^{-23}	-1.7×10^{-23}	-1.4×10^{-23}
$B(x_{\rm c})$	-7.5×10^{-39}	$-1. \times 10^{-39}$	5.7×10^{-40}	$2. \times 10^{-40}$	-1.1×10^{-39}
$U_1(x_{\rm c})$	1.9×10^{30}	4.1×10^{30}	2.8×10^{30}	3.5×10^{30}	1.1×10^{31}
$U_2(x_{\rm c})$	1.5×10^{34}	1.6×10^{34}	$2. \times 10^{34}$	2.4×10^{34}	3.4×10^{34}
$U_3(x_{\rm c})$	-9.6×10^{18}	-2.1×10^{19}	-1.3×10^{19}	-1.6×10^{19}	-4.4×10^{19}
$U_1(x_{\rm b})$	0.26	0.26	0.26	0.26	0.26
$U_2(x_{\rm b})$	7.4×10^{-18}	1.5×10^{-17}	7.4×10^{-18}	7.4×10^{-18}	1.5×10^{-17}
$U_3(x_{\rm b})$	8.9×10^{-17}	1.8×10^{-16}	8.9×10^{-17}	8.9×10^{-17}	1.8×10^{-16}
$V_1(x_{\rm c})$	0.00023	0.00047	0.00026	0.00027	0.00061
$V_2(x_{\rm c})$	$1. \times 10^{8}$	2.2×10^{8}	1.3×10^{8}	1.4×10^{8}	3.7×10^{8}
$V_3(x_{\rm c})$	-9.6×10^{18}	-2.1×10^{19}	-1.3×10^{19}	-1.6×10^{19}	-4.4×10^{19}
$V_1(x_{\rm b})$	8.4	8.4	8.4	8.4	8.4
$V_2(x_{\rm b})$	1.8×10^{-16}	3.6×10^{-16}	1.8×10^{-16}	1.8×10^{-16}	3.6×10^{-16}
$V_3(x_{\rm b})$	8.9×10^{-17}	1.8×10^{-16}	8.9×10^{-17}	8.9×10^{-17}	1.8×10^{-16}
$\alpha_{\rm c}$	2.553	2.553	2.553	2.553	2.553
θ_1^c	-2.357	-2.357	-2.357	-2.357	-2.357
θ_2^c	-0.5877	-0.5877	-0.5877	-0.5877	-0.5877
θ_3^c	0.7842	0.7842	0.7842	0.7842	0.7842
θ_4^c	2.554	2.554	2.554	2.554	2.554
μ_1^c	-0.5318	-0.5318	-0.5318	-0.5318	-0.5318
μ_2^c	1.597	1.597	1.597	1.597	1.597
μ_3^c	0.5318	0.5318	0.5318	0.5318	0.5318
μ_4^c	-1.597	-1.597	-1.597	-1.597	-1.597
$\alpha_{\rm q}$	-0.23	-0.23	-0.23	-0.23	-0.23
θ_1^q	-1.9	-1.9	-1.9	-1.9	-1.9
θ_2^q	-0.69	-0.69	-0.69	-0.69	-0.69
θ_3^q	1.2	1.2	1.2	1.2	1.2
θ_4^q	2.4	2.4	2.4	2.4	2.4
μ_1^q	-0.73	-0.73	-0.73	-0.73	-0.73
μ_2^q	1.1	1.1	1.1	1.1	1.1

Table 2 — *Continued.*

Characteristics	11	12	13	14	15
ϵ	2.4×10^{-23}	2.3×10^{-23}	2.2×10^{-23}	1.7×10^{-23}	1.5×10^{-23}
$x_{\rm b}$	0.5	0.5	0.5	0.5	0.5
$x_{\rm c}$	4.1×10^{11}	4.2×10^{11}	4.3×10^{11}	4.8×10^{11}	5.1×10^{11}
$A(x_{\rm b})$	-4.4×10^{-16}	-4.4×10^{-16}	-8.9×10^{-16}	-4.4×10^{-16}	-4.4×10^{-16}
$A(x_{\rm c})$	9.8×10^{-36}	9.1×10^{-36}	8.5×10^{-36}	$6.\times10^{-36}$	4.9×10^{-36}
$B(x_{\rm b})$	-1.2×10^{-23}	-1.1×10^{-23}	-1.1×10^{-23}	-8.6×10^{-24}	-7.6×10^{-24}
$B(x_{\rm c})$	-9.5×10^{-40}	2.4×10^{-39}	$-5.\times10^{-40}$	7.1×10^{-40}	-1.3×10^{-39}
$U_1(x_{\rm c})$	7.4×10^{30}	8.2×10^{30}	1.8×10^{31}	1.4×10^{31}	1.9×10^{31}
$U_2(x_{\rm c})$	4.2×10^{34}	4.5×10^{34}	4.8×10^{34}	6.9×10^{34}	8.4×10^{34}
$U_3(x_{\rm c})$	-2.7×10^{19}	-2.9×10^{19}	-6.3×10^{19}	-4.5×10^{19}	-5.4×10^{19}
$U_1(x_{\rm b})$	0.26	0.26	0.26	0.26	0.26
$U_2(x_{\rm b})$	7.4×10^{-18}	7.4×10^{-18}	1.5×10^{-17}	7.4×10^{-18}	7.4×10^{-18}
$U_3(x_{\rm b})$	8.9×10^{-17}	8.9×10^{-17}	1.8×10^{-16}	8.9×10^{-17}	8.9×10^{-17}
$V_1(x_{\rm c})$	0.00033	0.00033	0.00068	0.00038	0.00041
$V_2(x_{\rm c})$	2.1×10^{8}	2.2×10^{8}	4.6×10^{8}	2.9×10^{8}	3.3×10^{8}
$V_3(x_{\rm c})$	-2.7×10^{19}	-2.9×10^{19}	-6.3×10^{19}	-4.5×10^{19}	-5.4×10^{19}
$V_1(x_{\rm b})$	8.4	8.4	8.4	8.4	8.4
$V_2(x_{\rm b})$	1.8×10^{-16}	1.8×10^{-16}	3.6×10^{-16}	1.8×10^{-16}	1.8×10^{-16}
$V_3(x_{\rm b})$	8.9×10^{-17}	8.9×10^{-17}	1.8×10^{-16}	8.9×10^{-17}	8.9×10^{-17}
$\alpha_{\rm c}$	2.553	2.553	2.553	2.553	2.553
θ_1^c	-2.357	-2.357	-2.357	-2.357	-2.357
θ_2^c	-0.5877	-0.5877	-0.5877	-0.5877	-0.5877
θ_3^c	0.7842	0.7842	0.7842	0.7842	0.7842
θ_4^c	2.554	2.554	2.554	2.554	2.554
μ_1^c	-0.5318	-0.5318	-0.5318	-0.5318	-0.5318
μ_2^c	1.597	1.597	1.597	1.597	1.597
μ_3^c	0.5318	0.5318	0.5318	0.5318	0.5318
μ_4^c	-1.597	-1.597	-1.597	-1.597	-1.597
$\alpha_{\rm q}$	-0.23	-0.23	-0.23	-0.23	-0.23
θ_1^q	-1.9	-1.9	-1.9	-1.9	-1.9
θ_2^q	-0.69	-0.69	-0.69	-0.69	-0.69
θ_3^q	1.2	1.2	1.2	1.2	1.2
θ_4^q	2.4	2.4	2.4	2.4	2.4
μ_1^q	-0.73	-0.73	-0.73	-0.73	-0.73
μ_2^q	1.1	1.1	1.1	1.1	1.1

Characteristics	16	17	18	19	20
ϵ	1.5×10^{-23}	1.2×10^{-23}	1.2×10^{-23}	1.1×10^{-23}	$1.\times10^{-23}$
$x_{\rm b}$	0.5	0.5	0.5	0.5	0.5
$x_{\rm c}$	5.2×10^{11}	5.8×10^{11}	5.9×10^{11}	$6.\times10^{11}$	6.3×10^{11}
$A(x_{\rm b})$	-4.4×10^{-16}	-4.4×10^{-16}	-4.4×10^{-16}	-4.4×10^{-16}	-8.9×10^{-16}
$A(x_{\rm c})$	4.6×10^{-36}	3.5×10^{-36}	3.3×10^{-36}	3.2×10^{-36}	2.6×10^{-36}
$B(x_{\rm b})$	-7.3×10^{-24}	$-6.\times10^{-24}$	-5.8×10^{-24}	-5.6×10^{-24}	$-5.\times10^{-24}$
$B(x_{\rm c})$	4.7×10^{-40}	-1.7×10^{-39}	$-1.\times10^{-39}$	-7.4×10^{-40}	8.1×10^{-40}
$U_1(x_{\rm c})$	$2.\times10^{31}$	$3.\times10^{31}$	3.2×10^{31}	3.3×10^{31}	8.6×10^{31}
$U_2(x_{\rm c})$	8.9×10^{34}	1.2×10^{35}	1.3×10^{35}	1.3×10^{35}	1.6×10^{35}
$U_3(x_{\rm c})$	-5.8×10^{19}	-7.7×10^{19}	-8.2×10^{19}	-8.4×10^{19}	$-2.\times10^{20}$
$U_1(x_{\rm b})$	0.26	0.26	0.26	0.26	0.26
$U_2(x_{\rm b})$	7.4×10^{-18}	7.4×10^{-18}	7.4×10^{-18}	7.4×10^{-18}	1.5×10^{-17}
$U_3(x_{\rm b})$	8.9×10^{-17}	8.9×10^{-17}	8.9×10^{-17}	8.9×10^{-17}	1.8×10^{-16}
$V_1(x_{\rm c})$	0.00042	0.00046	0.00047	0.00048	0.001
$V_2(x_{\rm c})$	3.5×10^{8}	4.2×10^{8}	4.4×10^{8}	4.4×10^{8}	$1.\times10^{9}$
$V_3(x_{\rm c})$	-5.8×10^{19}	-7.7×10^{19}	-8.2×10^{19}	-8.4×10^{19}	$-2.\times10^{20}$
$V_1(x_{\rm b})$	8.4	8.4	8.4	8.4	8.4
$V_2(x_{\rm b})$	1.8×10^{-16}	1.8×10^{-16}	1.8×10^{-16}	1.8×10^{-16}	3.6×10^{-16}
$V_3(x_{\rm b})$	8.9×10^{-17}	8.9×10^{-17}	8.9×10^{-17}	8.9×10^{-17}	1.8×10^{-16}
$\alpha_{\rm c}$	2.553	2.553	2.553	2.553	2.553
θ_1^c	-2.357	-2.357	-2.357	-2.357	-2.357
θ_2^c	-0.5877	-0.5877	-0.5877	-0.5877	-0.5877
θ_3^c	0.7842	0.7842	0.7842	0.7842	0.7842
θ_4^c	2.554	2.554	2.554	2.554	2.554
μ_1^c	-0.5318	-0.5318	-0.5318	-0.5318	-0.5318
μ_2^c	1.597	1.597	1.597	1.597	1.597
μ_3^c	0.5318	0.5318	0.5318	0.5318	0.5318
μ_4^c	-1.597	-1.597	-1.597	-1.597	-1.597
$\alpha_{\rm q}$	-0.23	-0.23	-0.23	-0.23	-0.23
θ_1^q	-1.9	-1.9	-1.9	-1.9	-1.9
θ_2^q	-0.69	-0.69	-0.69	-0.69	-0.69
θ_3^q	1.2	1.2	1.2	1.2	1.2
θ_4^q	2.4	2.4	2.4	2.4	2.4
μ_1^q	-0.73	-0.73	-0.73	-0.73	-0.73
μ_2^q	1.1	1.1	1.1	1.1	1.1

Table 2 — *Continued.*

Characteristics	21	22	23	24	25
ϵ	7.3×10^{-24}	5.9×10^{-24}	$5.\times10^{-24}$	4.8×10^{-24}	4.8×10^{-24}
$x_{\rm b}$	0.5	0.5	0.5	0.5	0.5
$x_{\rm c}$	7.4×10^{11}	8.2×10^{11}	$9.\times10^{11}$	9.1×10^{11}	9.2×10^{11}
$A(x_{\rm b})$	-4.4×10^{-16}	-4.4×10^{-16}	-4.4×10^{-16}	-8.9×10^{-16}	-8.9×10^{-16}
$A(x_{\rm c})$	1.6×10^{-36}	1.2×10^{-36}	9.3×10^{-37}	8.7×10^{-37}	8.7×10^{-37}
$B(x_{\rm b})$	-3.7×10^{-24}	-2.9×10^{-24}	-2.5×10^{-24}	-2.4×10^{-24}	-2.4×10^{-24}
$B(x_{\rm c})$	2.4×10^{-40}	1.3×10^{-40}	2.3×10^{-40}	-2.6×10^{-40}	1.3×10^{-41}
$U_1(x_{\rm c})$	$8.\times10^{31}$	1.2×10^{32}	1.7×10^{32}	3.7×10^{32}	3.8×10^{32}
$U_2(x_{\rm c})$	2.5×10^{35}	3.5×10^{35}	4.4×10^{35}	4.7×10^{35}	4.7×10^{35}
$U_3(x_{\rm c})$	-1.6×10^{20}	-2.2×10^{20}	-2.9×10^{20}	-6.1×10^{20}	-6.2×10^{20}
$U_1(x_{\rm b})$	0.26	0.26	0.26	0.26	0.26
$U_2(x_{\rm b})$	7.4×10^{-18}	7.4×10^{-18}	7.4×10^{-18}	1.5×10^{-17}	1.5×10^{-17}
$U_3(x_{\rm b})$	8.9×10^{-17}	8.9×10^{-17}	8.9×10^{-17}	1.8×10^{-16}	1.8×10^{-16}
$V_1(x_{\rm c})$	0.00059	0.00066	0.00072	0.0015	0.0015
$V_2(x_{\rm c})$	6.9×10^{8}	8.5×10^{8}	$1.\times10^{9}$	2.1×10^{9}	2.1×10^{9}
$V_3(x_{\rm c})$	-1.6×10^{20}	-2.2×10^{20}	-2.9×10^{20}	-6.1×10^{20}	-6.2×10^{20}
$V_1(x_{\rm b})$	8.4	8.4	8.4	8.4	8.4
$V_2(x_{\rm b})$	1.8×10^{-16}	1.8×10^{-16}	1.8×10^{-16}	3.6×10^{-16}	3.6×10^{-16}
$V_3(x_{\rm b})$	8.9×10^{-17}	8.9×10^{-17}	8.9×10^{-17}	1.8×10^{-16}	1.8×10^{-16}
$\alpha_{\rm c}$	2.553	2.553	2.553	2.553	2.553
θ_1^c	-2.357	-2.357	-2.357	-2.357	-2.357
θ_2^c	-0.5877	-0.5877	-0.5877	-0.5877	-0.5877
θ_3^c	0.7842	0.7842	0.7842	0.7842	0.7842
θ_4^c	2.554	2.554	2.554	2.554	2.554
μ_1^c	-0.5318	-0.5318	-0.5318	-0.5318	-0.5318
μ_2^c	1.597	1.597	1.597	1.597	1.597
μ_3^c	0.5318	0.5318	0.5318	0.5318	0.5318
μ_4^c	-1.597	-1.597	-1.597	-1.597	-1.597
$\alpha_{\rm q}$	-0.23	-0.23	-0.23	-0.23	-0.23
θ_1^q	-1.9	-1.9	-1.9	-1.9	-1.9
θ_2^q	-0.69	-0.69	-0.69	-0.69	-0.69
θ_3^q	1.2	1.2	1.2	1.2	1.2
θ_4^q	2.4	2.4	2.4	2.4	2.4
μ_1^q	-0.73	-0.73	-0.73	-0.73	-0.73
μ_2^q	1.1	1.1	1.1	1.1	1.1
Characteristics	26	27	28	29	30
ϵ	3.3×10^{-24}	3.2×10^{-24}	$3.\times10^{-24}$	2.7×10^{-24}	2.4×10^{-24}
$x_{\rm b}$	0.5	0.5	0.5	0.5	0.5
$x_{\rm c}$	1.1×10^{12}	1.1×10^{12}	1.2×10^{12}	1.2×10^{12}	1.3×10^{12}
$A(x_{\rm b})$	-4.4×10^{-16}	-8.9×10^{-16}	-4.4×10^{-16}	-8.9×10^{-16}	-4.4×10^{-16}
$A(x_{\rm c})$	$5.\times10^{-37}$	4.7×10^{-37}	4.3×10^{-37}	3.6×10^{-37}	3.2×10^{-37}
$B(x_{\rm b})$	-1.7×10^{-24}	-1.6×10^{-24}	-1.5×10^{-24}	-1.3×10^{-24}	-1.2×10^{-24}
$B(x_{\rm c})$	9.9×10^{-41}	4.2×10^{-41}	-4.8×10^{-40}	2.9×10^{-40}	1.9×10^{-40}
$U_1(x_{\rm c})$	3.9×10^{32}	8.5×10^{32}	4.7×10^{32}	1.2×10^{33}	7.2×10^{32}
$U_2(x_{\rm c})$	8.2×10^{35}	8.8×10^{35}	9.5×10^{35}	1.1×10^{36}	1.3×10^{36}
$U_3(x_{\rm c})$	-5.3×10^{20}	-1.1×10^{21}	-6.2×10^{20}	-1.5×10^{21}	-8.4×10^{20}
$U_1(x_{\rm b})$	0.26	0.26	0.26	0.26	0.26
$U_2(x_{\rm b})$	7.4×10^{-18}	1.5×10^{-17}	7.4×10^{-18}	1.5×10^{-17}	7.4×10^{-18}
$U_3(x_{\rm b})$	8.9×10^{-17}	1.8×10^{-16}	8.9×10^{-17}	1.8×10^{-16}	8.9×10^{-17}
$V_1(x_{\rm c})$	0.00088	0.0018	0.00092	0.002	0.001
$V_2(x_{\rm c})$	1.5×10^{9}	3.2×10^{9}	1.7×10^{9}	3.8×10^{9}	2.1×10^{9}
$V_3(x_{\rm c})$	-5.3×10^{20}	-1.1×10^{21}	-6.2×10^{20}	-1.5×10^{21}	-8.4×10^{20}
$V_1(x_{\rm b})$	8.4	8.4	8.4	8.4	8.4
$V_2(x_{\rm b})$	1.8×10^{-16}	3.6×10^{-16}	1.8×10^{-16}	3.6×10^{-16}	1.8×10^{-16}
$V_3(x_{\rm b})$	8.9×10^{-17}	1.8×10^{-16}	8.9×10^{-17}	1.8×10^{-16}	8.9×10^{-17}
$\alpha_{\rm c}$	2.553	2.553	2.553	2.553	2.553
θ_1^c	-2.357	-2.357	-2.357	-2.357	-2.357
θ_2^c	-0.5877	-0.5877	-0.5877	-0.5877	-0.5877
θ_3^c	0.7842	0.7842	0.7842	0.7842	0.7842
θ_4^c	2.554	2.554	2.554	2.554	2.554
μ_1^c	-0.5318	-0.5318	-0.5318	-0.5318	-0.5318
μ_2^c	1.597	1.597	1.597	1.597	1.597
μ_3^c	0.5318	0.5318	0.5318	0.5318	0.5318
μ_4^c	-1.597	-1.597	-1.597	-1.597	-1.597
$\alpha_{\rm q}$	-0.23	-0.23	-0.23	-0.23	-0.23
θ_1^q	-1.9	-1.9	-1.9	-1.9	-1.9
θ_2^q	-0.69	-0.69	-0.69	-0.69	-0.69
θ_3^q	1.2	1.2	1.2	1.2	1.2
θ_4^q	2.4	2.4	2.4	2.4	2.4
μ_1^q	-0.73	-0.73	-0.73	-0.73	-0.73
μ_2^q	1.1	1.1	1.1	1.1	1.1

Table 2 — *Continued.*

Characteristics	31	32	33	34	35
ϵ	$2.\times10^{-24}$	1.9×10^{-24}	1.5×10^{-24}	1.4×10^{-24}	1.2×10^{-24}
$x_{\rm b}$	0.5	0.5	0.5	0.5	0.5
$x_{\rm c}$	1.4×10^{12}	1.4×10^{12}	1.6×10^{12}	1.7×10^{12}	1.9×10^{12}
$A(x_{\rm b})$	-4.4×10^{-16}	-4.4×10^{-16}	-8.9×10^{-16}	-4.4×10^{-16}	-8.9×10^{-16}
$A(x_{\rm c})$	2.4×10^{-37}	2.2×10^{-37}	1.5×10^{-37}	1.4×10^{-37}	$1.\times10^{-37}$
$B(x_{\rm b})$	$-1.\times10^{-24}$	-9.6×10^{-25}	-7.3×10^{-25}	-6.9×10^{-25}	-5.8×10^{-25}
$B(x_{\rm c})$	-1.1×10^{-40}	1.5×10^{-40}	1.6×10^{-41}	1.2×10^{-40}	$-2.\times10^{-41}$
$U_1(x_{\rm c})$	$1.\times10^{33}$	1.2×10^{33}	3.9×10^{33}	2.2×10^{33}	6.4×10^{33}
$U_2(x_{\rm c})$	1.7×10^{36}	1.9×10^{36}	2.8×10^{36}	$3.\times10^{36}$	$4.\times10^{36}$
$U_3(x_{\rm c})$	-1.1×10^{21}	-1.2×10^{21}	-3.6×10^{21}	$-2.\times10^{21}$	-5.2×10^{21}
$U_1(x_{\rm b})$	0.26	0.26	0.26	0.26	0.26
$U_2(x_{\rm b})$	7.4×10^{-18}	7.4×10^{-18}	1.5×10^{-17}	7.4×10^{-18}	1.5×10^{-17}
$U_3(x_{\rm b})$	8.9×10^{-17}	8.9×10^{-17}	1.8×10^{-16}	8.9×10^{-17}	1.8×10^{-16}
$V_1(x_{\rm c})$	0.0011	0.0012	0.0026	0.0014	0.003
$V_2(x_{\rm c})$	2.5×10^{9}	2.6×10^{9}	6.8×10^{9}	3.6×10^{9}	8.7×10^{9}
$V_3(x_{\rm c})$	-1.1×10^{21}	-1.2×10^{21}	-3.6×10^{21}	$-2.\times10^{21}$	-5.2×10^{21}
$V_1(x_{\rm b})$	8.4	8.4	8.4	8.4	8.4
$V_2(x_{\rm b})$	1.8×10^{-16}	1.8×10^{-16}	3.6×10^{-16}	1.8×10^{-16}	3.6×10^{-16}
$V_3(x_{\rm b})$	8.9×10^{-17}	8.9×10^{-17}	1.8×10^{-16}	8.9×10^{-17}	1.8×10^{-16}
$\alpha_{\rm c}$	2.553	2.553	2.553	2.553	2.553
θ_1^c	-2.357	-2.357	-2.357	-2.357	-2.357
θ_2^c	-0.5877	-0.5877	-0.5877	-0.5877	-0.5877
θ_3^c	0.7842	0.7842	0.7842	0.7842	0.7842
θ_4^c	2.554	2.554	2.554	2.554	2.554
μ_1^c	-0.5318	-0.5318	-0.5318	-0.5318	-0.5318
μ_2^c	1.597	1.597	1.597	1.597	1.597
μ_3^c	0.5318	0.5318	0.5318	0.5318	0.5318
μ_4^c	-1.597	-1.597	-1.597	-1.597	-1.597
$\alpha_{\rm q}$	-0.23	-0.23	-0.23	-0.23	-0.23
θ_1^q	-1.9	-1.9	-1.9	-1.9	-1.9
θ_2^q	-0.69	-0.69	-0.69	-0.69	-0.69
θ_3^q	1.2	1.2	1.2	1.2	1.2
θ_4^q	2.4	2.4	2.4	2.4	2.4
μ_1^q	-0.73	-0.73	-0.73	-0.73	-0.73
μ_2^q	1.1	1.1	1.1	1.1	1.1
Characteristics	36	37	38	39	40
ϵ	1.1×10^{-24}	8.3×10^{-25}	6.9×10^{-25}	$6.\times10^{-25}$	4.8×10^{-25}
$x_{\rm b}$	0.5	0.5	0.5	0.5	0.5
$x_{\rm c}$	1.9×10^{12}	2.2×10^{12}	2.4×10^{12}	2.6×10^{12}	2.9×10^{12}
$A(x_{\rm b})$	-4.4×10^{-16}	-4.4×10^{-16}	-4.4×10^{-16}	-4.4×10^{-16}	-4.4×10^{-16}
$A(x_{\rm c})$	9.4×10^{-38}	6.3×10^{-38}	4.8×10^{-38}	3.9×10^{-38}	2.8×10^{-38}
$B(x_{\rm b})$	-5.4×10^{-25}	-4.2×10^{-25}	-3.5×10^{-25}	$-3.\times10^{-25}$	-2.4×10^{-25}
$B(x_{\rm c})$	5.7×10^{-41}	3.8×10^{-41}	-3.3×10^{-41}	1.1×10^{-41}	1.9×10^{-41}
$U_1(x_{\rm c})$	3.7×10^{33}	6.2×10^{33}	8.9×10^{33}	1.2×10^{34}	1.9×10^{34}
$U_2(x_{\rm c})$	4.4×10^{36}	6.5×10^{36}	8.6×10^{36}	1.1×10^{37}	1.5×10^{37}
$U_3(x_{\rm c})$	-2.8×10^{21}	-4.2×10^{21}	-5.6×10^{21}	-6.8×10^{21}	-9.6×10^{21}
$U_1(x_{\rm b})$	0.26	0.26	0.26	0.26	0.26
$U_2(x_{\rm b})$	7.4×10^{-18}	7.4×10^{-18}	7.4×10^{-18}	7.4×10^{-18}	7.4×10^{-18}
$U_3(x_{\rm b})$	8.9×10^{-17}	8.9×10^{-17}	8.9×10^{-17}	8.9×10^{-17}	8.9×10^{-17}
$V_1(x_{\rm c})$	0.0015	0.0018	0.0019	0.0021	0.0023
$V_2(x_{\rm c})$	4.7×10^{9}	6.1×10^{9}	7.3×10^{9}	8.3×10^{9}	$1.\times10^{10}$
$V_3(x_{\rm c})$	-2.8×10^{21}	-4.2×10^{21}	-5.6×10^{21}	-6.8×10^{21}	-9.6×10^{21}
$V_1(x_{\rm b})$	8.4	8.4	8.4	8.4	8.4
$V_2(x_{\rm b})$	1.8×10^{-16}	1.8×10^{-16}	1.8×10^{-16}	1.8×10^{-16}	1.8×10^{-16}
$V_3(x_{\rm b})$	8.9×10^{-17}	8.9×10^{-17}	8.9×10^{-17}	8.9×10^{-17}	8.9×10^{-17}
$\alpha_{\rm c}$	2.553	2.553	2.553	2.553	2.553
θ_1^c	-2.357	-2.357	-2.357	-2.357	-2.357
θ_2^c	-0.5877	-0.5877	-0.5877	-0.5877	-0.5877
θ_3^c	0.7842	0.7842	0.7842	0.7842	0.7842
θ_4^c	2.554	2.554	2.554	2.554	2.554
μ_1^c	-0.5318	-0.5318	-0.5318	-0.5318	-0.5318
μ_2^c	1.597	1.597	1.597	1.597	1.597
μ_3^c	0.5318	0.5318	0.5318	0.5318	0.5318
μ_4^c	-1.597	-1.597	-1.597	-1.597	-1.597
$\alpha_{\rm q}$	-0.23	-0.23	-0.23	-0.23	-0.23
θ_1^q	-1.9	-1.9	-1.9	-1.9	-1.9
θ_2^q	-0.69	-0.69	-0.69	-0.69	-0.69
θ_3^q	1.2	1.2	1.2	1.2	1.2
θ_4^q	2.4	2.4	2.4	2.4	2.4
μ_1^q	-0.73	-0.73	-0.73	-0.73	-0.73
μ_2^q	1.1	1.1	1.1	1.1	1.1

Table 2 — *Continued.*

Characteristics	41	42	43	44	45
ϵ	2.7×10^{-25}	1.2×10^{-25}	9.7×10^{-26}	1.9×10^{-26}	1.5×10^{-26}
$x_{\rm b}$	0.5	0.5	0.5	0.5	0.5
$x_{\rm c}$	3.8×10^{12}	5.8×10^{12}	6.4×10^{12}	1.4×10^{13}	1.6×10^{13}
$A(x_{\rm b})$	-8.9×10^{-16}	-4.4×10^{-16}	-4.4×10^{-16}	-4.4×10^{-16}	-8.9×10^{-16}
$A(x_{\rm c})$	1.2×10^{-38}	3.5×10^{-39}	2.5×10^{-39}	2.2×10^{-40}	1.5×10^{-40}
$B(x_{\rm b})$	-1.3×10^{-25}	$-6.\times10^{-26}$	-4.9×10^{-26}	-9.6×10^{-27}	-7.3×10^{-27}
$B(x_{\rm c})$	-1.6×10^{-41}	$2.\times10^{-41}$	-5.3×10^{-42}	$7.\times10^{-43}$	-7.4×10^{-43}
$U_1(x_{\rm c})$	1.2×10^{35}	$3.\times10^{35}$	4.5×10^{35}	1.2×10^{37}	3.9×10^{37}
$U_2(x_{\rm c})$	3.5×10^{37}	1.2×10^{38}	1.6×10^{38}	1.9×10^{39}	2.8×10^{39}
$U_3(x_{\rm c})$	-4.6×10^{22}	-7.7×10^{22}	-1.1×10^{23}	-1.2×10^{24}	-3.6×10^{24}
$U_1(x_{\rm b})$	0.26	0.26	0.26	0.26	0.26
$U_2(x_{\rm b})$	1.5×10^{-17}	7.4×10^{-18}	7.4×10^{-18}	7.4×10^{-18}	1.5×10^{-17}
$U_3(x_{\rm b})$	1.8×10^{-16}	8.9×10^{-17}	8.9×10^{-17}	8.9×10^{-17}	1.8×10^{-16}
$V_1(x_{\rm c})$	0.0062	0.0046	0.0051	0.012	0.026
$V_2(x_{\rm c})$	3.7×10^{10}	4.2×10^{10}	5.2×10^{10}	2.6×10^{11}	6.8×10^{11}
$V_3(x_{\rm c})$	-4.6×10^{22}	-7.7×10^{22}	-1.1×10^{23}	-1.2×10^{24}	-3.6×10^{24}
$V_1(x_{\rm b})$	8.4	8.4	8.4	8.4	8.4
$V_2(x_{\rm b})$	3.6×10^{-16}	1.8×10^{-16}	1.8×10^{-16}	1.8×10^{-16}	3.6×10^{-16}
$V_3(x_{\rm b})$	1.8×10^{-16}	8.9×10^{-17}	8.9×10^{-17}	8.9×10^{-17}	1.8×10^{-16}
$\alpha_{\rm c}$	2.553	2.553	2.553	2.553	2.553
θ_1^c	-2.357	-2.357	-2.357	-2.357	-2.357
θ_2^c	-0.5877	-0.5877	-0.5877	-0.5877	-0.5877
θ_3^c	0.7842	0.7842	0.7842	0.7842	0.7842
θ_4^c	2.554	2.554	2.554	2.554	2.554
μ_1^c	-0.5318	-0.5318	-0.5318	-0.5318	-0.5318
μ_2^c	1.597	1.597	1.597	1.597	1.597
μ_3^c	0.5318	0.5318	0.5318	0.5318	0.5318
μ_4^c	-1.597	-1.597	-1.597	-1.597	-1.597
$\alpha_{\rm q}$	-0.23	-0.23	-0.23	-0.23	-0.23
θ_1^q	-1.9	-1.9	-1.9	-1.9	-1.9
θ_2^q	-0.69	-0.69	-0.69	-0.69	-0.69
θ_3^q	1.2	1.2	1.2	1.2	1.2
θ_4^q	2.4	2.4	2.4	2.4	2.4
μ_1^q	-0.73	-0.73	-0.73	-0.73	-0.73
μ_2^q	1.1	1.1	1.1	1.1	1.1
Characteristics	46	47	48	49	50
ϵ	1.4×10^{-26}	8.7×10^{-27}	6.3×10^{-27}	1.2×10^{-27}	7.7×10^{-28}
$x_{\rm b}$	0.5	0.5	0.5	0.5	0.5
$x_{\rm c}$	1.7×10^{13}	2.1×10^{13}	2.5×10^{13}	5.8×10^{13}	7.2×10^{13}
$A(x_{\rm b})$	-8.9×10^{-16}	-8.9×10^{-16}	-4.4×10^{-16}	-4.4×10^{-16}	-4.4×10^{-16}
$A(x_{\rm c})$	1.4×10^{-40}	6.8×10^{-41}	4.2×10^{-41}	3.5×10^{-42}	1.8×10^{-42}
$B(x_{\rm b})$	-6.9×10^{-27}	-4.4×10^{-27}	-3.2×10^{-27}	$-6.\times10^{-28}$	-3.8×10^{-28}
$B(x_{\rm c})$	-9.4×10^{-43}	6.4×10^{-43}	-1.7×10^{-43}	$1.\times10^{-43}$	$6.\times10^{-44}$
$U_1(x_{\rm c})$	4.4×10^{37}	1.1×10^{38}	1.1×10^{38}	$3.\times10^{39}$	7.2×10^{39}
$U_2(x_{\rm c})$	$3.\times10^{39}$	$6.\times10^{39}$	9.8×10^{39}	1.2×10^{41}	2.3×10^{41}
$U_3(x_{\rm c})$	-3.9×10^{24}	-7.8×10^{24}	-6.3×10^{24}	-7.7×10^{25}	-1.5×10^{26}
$U_1(x_{\rm b})$	0.26	0.26	0.26	0.26	0.26
$U_2(x_{\rm b})$	1.5×10^{-17}	1.5×10^{-17}	7.4×10^{-18}	7.4×10^{-18}	7.4×10^{-18}
$U_3(x_{\rm b})$	1.8×10^{-16}	1.8×10^{-16}	8.9×10^{-17}	8.9×10^{-17}	8.9×10^{-17}
$V_1(x_{\rm c})$	0.027	0.034	0.02	0.046	0.058
$V_2(x_{\rm c})$	7.2×10^{11}	1.1×10^{12}	7.9×10^{11}	4.2×10^{12}	6.5×10^{12}
$V_3(x_{\rm c})$	-3.9×10^{24}	-7.8×10^{24}	-6.3×10^{24}	-7.7×10^{25}	-1.5×10^{26}
$V_1(x_{\rm b})$	8.4	8.4	8.4	8.4	8.4
$V_2(x_{\rm b})$	3.6×10^{-16}	3.6×10^{-16}	1.8×10^{-16}	1.8×10^{-16}	1.8×10^{-16}
$V_3(x_{\rm b})$	1.8×10^{-16}	1.8×10^{-16}	8.9×10^{-17}	8.9×10^{-17}	8.9×10^{-17}
$\alpha_{\rm c}$	2.553	2.553	2.553	2.553	2.553
θ_1^c	-2.357	-2.357	-2.357	-2.357	-2.357
θ_2^c	-0.5877	-0.5877	-0.5877	-0.5877	-0.5877
θ_3^c	0.7842	0.7842	0.7842	0.7842	0.7842
θ_4^c	2.554	2.554	2.554	2.554	2.554
μ_1^c	-0.5318	-0.5318	-0.5318	-0.5318	-0.5318
μ_2^c	1.597	1.597	1.597	1.597	1.597
μ_3^c	0.5318	0.5318	0.5318	0.5318	0.5318
μ_4^c	-1.597	-1.597	-1.597	-1.597	-1.597
$\alpha_{\rm q}$	-0.23	-0.23	-0.23	-0.23	-0.23
θ_1^q	-1.9	-1.9	-1.9	-1.9	-1.9
θ_2^q	-0.69	-0.69	-0.69	-0.69	-0.69
θ_3^q	1.2	1.2	1.2	1.2	1.2
θ_4^q	2.4	2.4	2.4	2.4	2.4
μ_1^q	-0.73	-0.73	-0.73	-0.73	-0.73
μ_2^q	1.1	1.1	1.1	1.1	1.1

Table 2 — *Continued.*

Characteristics	51	52	53	54	55
ϵ	5.9×10^{-28}	3.6×10^{-28}	2.8×10^{-28}	1.9×10^{-28}	1.1×10^{-28}
$x_{\rm b}$	0.5	0.5	0.5	0.5	0.5
$x_{\rm c}$	8.2×10^{13}	$1.\times10^{14}$	1.2×10^{14}	1.4×10^{14}	1.9×10^{14}
$A(x_{\rm b})$	-4.4×10^{-16}	-8.9×10^{-16}	-4.4×10^{-16}	-4.4×10^{-16}	-4.4×10^{-16}
$A(x_{\rm c})$	1.2×10^{-42}	5.8×10^{-43}	3.8×10^{-43}	2.2×10^{-43}	9.4×10^{-44}
$B(x_{\rm b})$	-2.9×10^{-28}	-1.8×10^{-28}	-1.4×10^{-28}	-9.6×10^{-29}	-5.4×10^{-29}
$B(x_{\rm c})$	-2.2×10^{-44}	-4.7×10^{-44}	3.9×10^{-44}	$3.\times10^{-44}$	-1.2×10^{-44}
$U_1(x_{\rm c})$	1.2×10^{40}	6.5×10^{40}	5.6×10^{40}	1.2×10^{41}	3.7×10^{41}
$U_2(x_{\rm c})$	3.5×10^{41}	7.1×10^{41}	1.1×10^{42}	1.9×10^{42}	4.4×10^{42}
$U_3(x_{\rm c})$	-2.2×10^{26}	-9.2×10^{26}	$-7.\times10^{26}$	-1.2×10^{27}	-2.8×10^{27}
$U_1(x_{\rm b})$	0.26	0.26	0.26	0.26	0.26
$U_2(x_{\rm b})$	7.4×10^{-18}	1.5×10^{-17}	7.4×10^{-18}	7.4×10^{-18}	7.4×10^{-18}
$U_3(x_{\rm b})$	8.9×10^{-17}	1.8×10^{-16}	8.9×10^{-17}	8.9×10^{-17}	8.9×10^{-17}
$V_1(x_{\rm c})$	0.066	0.17	0.096	0.12	0.15
$V_2(x_{\rm c})$	8.5×10^{12}	2.8×10^{13}	1.8×10^{13}	2.6×10^{13}	4.7×10^{13}
$V_3(x_{\rm c})$	-2.2×10^{26}	-9.2×10^{26}	$-7.\times10^{26}$	-1.2×10^{27}	-2.8×10^{27}
$V_1(x_{\rm b})$	8.4	8.4	8.4	8.4	8.4
$V_2(x_{\rm b})$	1.8×10^{-16}	3.6×10^{-16}	1.8×10^{-16}	1.8×10^{-16}	1.8×10^{-16}
$V_3(x_{\rm b})$	8.9×10^{-17}	1.8×10^{-16}	8.9×10^{-17}	8.9×10^{-17}	8.9×10^{-17}
$\alpha_{\rm c}$	2.553	2.553	2.553	2.553	2.553
θ_1^c	-2.357	-2.357	-2.357	-2.357	-2.357
θ_2^c	-0.5877	-0.5877	-0.5877	-0.5877	-0.5877
θ_3^c	0.7842	0.7842	0.7842	0.7842	0.7842
θ_4^c	2.554	2.554	2.554	2.554	2.554
μ_1^c	-0.5318	-0.5318	-0.5318	-0.5318	-0.5318
μ_2^c	1.597	1.597	1.597	1.597	1.597
μ_3^c	0.5318	0.5318	0.5318	0.5318	0.5318
μ_4^c	-1.597	-1.597	-1.597	-1.597	-1.597
$\alpha_{\rm q}$	-0.23	-0.23	-0.23	-0.23	-0.23
θ_1^q	-1.9	-1.9	-1.9	-1.9	-1.9
θ_2^q	-0.69	-0.69	-0.69	-0.69	-0.69
θ_3^q	1.2	1.2	1.2	1.2	1.2
θ_4^q	2.4	2.4	2.4	2.4	2.4
μ_1^q	-0.73	-0.73	-0.73	-0.73	-0.73
μ_2^q	1.1	1.1	1.1	1.1	1.1
Characteristics	56	57	58	59	60
ϵ	6.9×10^{-31}	4.8×10^{-29}	1.2×10^{-29}	$3.\times10^{-30}$	2.2×10^{-30}
$x_{\rm b}$	0.5	0.5	0.5	0.5	0.5
$x_{\rm c}$	2.4×10^{15}	2.9×10^{14}	5.8×10^{14}	1.2×10^{15}	1.3×10^{15}
$A(x_{\rm b})$	-8.9×10^{-16}	-4.4×10^{-16}	-4.4×10^{-16}	-4.4×10^{-16}	-4.4×10^{-16}
$A(x_{\rm c})$	4.8×10^{-47}	2.8×10^{-44}	3.5×10^{-45}	4.3×10^{-46}	2.8×10^{-46}
$B(x_{\rm b})$	-3.5×10^{-31}	-2.4×10^{-29}	$-6.\times10^{-30}$	-1.5×10^{-30}	-1.1×10^{-30}
$B(x_{\rm c})$	7.5×10^{-47}	6.5×10^{-45}	2.2×10^{-45}	4.5×10^{-46}	$-3.\times10^{-46}$
$U_1(x_{\rm c})$	1.8×10^{46}	1.9×10^{42}	$3.\times10^{43}$	4.7×10^{44}	8.7×10^{44}
$U_2(x_{\rm c})$	8.6×10^{45}	1.5×10^{43}	1.2×10^{44}	9.5×10^{44}	1.5×10^{45}
$U_3(x_{\rm c})$	-1.1×10^{31}	-9.6×10^{27}	-7.7×10^{28}	-6.2×10^{29}	-9.7×10^{29}
$U_1(x_{\rm b})$	0.26	0.26	0.26	0.26	0.26
$U_2(x_{\rm b})$	1.5×10^{-17}	7.4×10^{-18}	7.4×10^{-18}	7.4×10^{-18}	7.4×10^{-18}
$U_3(x_{\rm b})$	1.8×10^{-16}	8.9×10^{-17}	8.9×10^{-17}	8.9×10^{-17}	8.9×10^{-17}
$V_1(x_{\rm c})$	3.8	0.23	0.46	0.92	1.1
$V_2(x_{\rm c})$	1.5×10^{16}	$1.\times10^{14}$	4.2×10^{14}	1.7×10^{15}	2.3×10^{15}
$V_3(x_{\rm c})$	-1.1×10^{31}	-9.6×10^{27}	-7.7×10^{28}	-6.2×10^{29}	-9.7×10^{29}
$V_1(x_{\rm b})$	8.4	8.4	8.4	8.4	8.4
$V_2(x_{\rm b})$	3.6×10^{-16}	1.8×10^{-16}	1.8×10^{-16}	1.8×10^{-16}	1.8×10^{-16}
$V_3(x_{\rm b})$	1.8×10^{-16}	8.9×10^{-17}	8.9×10^{-17}	8.9×10^{-17}	8.9×10^{-17}
$\alpha_{\rm c}$	2.553	2.553	2.553	2.553	2.553
θ_1^c	-2.357	-2.357	-2.357	-2.357	-2.357
θ_2^c	-0.5877	-0.5877	-0.5877	-0.5877	-0.5877
θ_3^c	0.7842	0.7842	0.7842	0.7842	0.7842
θ_4^c	2.554	2.554	2.554	2.554	2.554
μ_1^c	-0.5318	-0.5318	-0.5318	-0.5318	-0.5318
μ_2^c	1.597	1.597	1.597	1.597	1.597
μ_3^c	0.5318	0.5318	0.5318	0.5318	0.5318
μ_4^c	-1.597	-1.597	-1.597	-1.597	-1.597
$\alpha_{\rm q}$	-0.23	-0.23	-0.23	-0.23	-0.23
θ_1^q	-1.9	-1.9	-1.9	-1.9	-1.9
θ_2^q	-0.69	-0.69	-0.69	-0.69	-0.69
θ_3^q	1.2	1.2	1.2	1.2	1.2
θ_4^q	2.4	2.4	2.4	2.4	2.4
μ_1^q	-0.73	-0.73	-0.73	-0.73	-0.73
μ_2^q	1.1	1.1	1.1	1.1	1.1

Table 3 Real Quantum Deflection Angle Calculated Values for $0.001 < \epsilon < 0.01$ where $\mu_3 = -\mu_1, \mu_4 = -\mu_2$

ϵ	α_q	θ_1	θ_2	θ_3	θ_4	μ_1	μ_2
0.0022	–0.598212	–2.36947	–0.584932	0.772118	2.55666	–0.525425	1.62159
0.0023	–0.598235	–2.3695	–0.584925	0.772088	2.55667	–0.52541	1.62165
0.0025	–0.598299	–2.36959	–0.584905	0.772004	2.55669	–0.525365	1.62183
0.0026	–0.59834	–2.36964	–0.584893	0.771951	2.5567	–0.525337	1.62194
0.0027	–0.598386	–2.3697	–0.584879	0.771891	2.55671	–0.525306	1.62207
0.0028	–0.598437	–2.36977	–0.584864	0.771825	2.55673	–0.525271	1.6222
0.0029	–0.598492	–2.36984	–0.584847	0.771753	2.55675	–0.525233	1.62235
0.0030	–0.598552	–2.36992	–0.584829	0.771675	2.55676	–0.525192	1.62252
0.0031	–0.598615	–2.37	–0.58481	0.771593	2.55678	–0.525148	1.62269
0.0032	–0.598703	–2.37011	–0.584783	0.771479	2.55681	–0.525088	1.62293
0.0033	–0.598753	–2.37018	–0.584768	0.771413	2.55682	–0.525053	1.62307
0.0034	–0.598827	–2.37028	–0.584746	0.771317	2.55685	–0.525002	1.62327
0.0035	–0.598904	–2.37038	–0.584722	0.771216	2.55687	–0.524949	1.62348
0.0036	–0.598985	–2.37048	–0.584698	0.771112	2.55689	–0.524894	1.6237
0.0037	–0.599068	–2.37059	–0.584673	0.771004	2.55692	–0.524837	1.62392
0.0038	–0.599153	–2.3707	–0.584647	0.770892	2.55695	–0.524778	1.62416
0.0040	–0.599332	–2.37093	–0.584593	0.77066	2.557	–0.524655	1.62465
0.0044	–0.599716	–2.37143	–0.584478	0.77016	2.55712	–0.524392	1.6257
0.0045	–0.599816	–2.37156	–0.584447	0.770029	2.55715	–0.524322	1.62597
0.0046	–0.599919	–2.3717	–0.584416	0.769896	2.55718	–0.524252	1.62626
0.0047	–0.600023	–2.37183	–0.584385	0.76976	2.55721	–0.52418	1.62654
0.0048	–0.600129	–2.37197	–0.584353	0.769622	2.55724	–0.524107	1.62683
0.0049	–0.600236	–2.37211	–0.584321	0.769483	2.55727	–0.524033	1.62713
0.0050	–0.600345	–2.37225	–0.584288	0.769341	2.5573	–0.523959	1.62743
0.0051	–0.600455	–2.37239	–0.584254	0.769198	2.55734	–0.523883	1.62773
0.0053	–0.600678	–2.37269	–0.584187	0.768907	2.55741	–0.523729	1.62835
0.0054	–0.600792	–2.37283	–0.584153	0.768759	2.55744	–0.523651	1.62866
0.0058	–0.601266	–2.37345	–0.584009	0.768142	2.55758	–0.523324	1.62997
0.0059	–0.601375	–2.37359	–0.583976	0.768	2.55762	–0.523249	1.63027
0.0062	–0.601734	–2.37406	–0.583868	0.767532	2.55772	–0.523001	1.63127
0.0064	–0.601977	–2.37438	–0.583794	0.767215	2.5578	–0.522834	1.63194
0.0065	–0.602099	–2.37454	–0.583757	0.767056	2.55784	–0.522749	1.63228
0.0066	–0.602222	–2.3747	–0.58372	0.766896	2.55787	–0.522665	1.63262
0.0067	–0.602345	–2.37486	–0.583683	0.766736	2.55791	–0.52258	1.63297
0.0068	–0.602469	–2.37502	–0.583646	0.766575	2.55795	–0.522494	1.63331
0.0069	–0.602593	–2.37518	–0.583608	0.766414	2.55798	–0.522409	1.63366
0.0070	–0.602717	–2.37534	–0.583571	0.766252	2.55802	–0.522323	1.634
0.0071	–0.602841	–2.3755	–0.583533	0.76609	2.55806	–0.522237	1.63435
0.0073	–0.60309	–2.37583	–0.583458	0.765765	2.55813	–0.522065	1.63505
0.0074	–0.603215	–2.37599	–0.58342	0.765603	2.55817	–0.521979	1.6354
0.0075	–0.60334	–2.37615	–0.583382	0.765441	2.55821	–0.521893	1.63575
0.0079	–0.603838	–2.3768	–0.583232	0.764792	2.55836	–0.521549	1.63714
0.0080	–0.603961	–2.37696	–0.583194	0.764631	2.5584	–0.521463	1.63749
0.0081	–0.604085	–2.37712	–0.583157	0.76447	2.55844	–0.521378	1.63784
0.0085	–0.604574	–2.37776	–0.583009	0.763834	2.55858	–0.52104	1.63922
0.0086	–0.604694	–2.37792	–0.582972	0.763676	2.55862	–0.520957	1.63956
0.0091	–0.60528	–2.37868	–0.582795	0.762914	2.5588	–0.520551	1.64122
0.0092	–0.605393	–2.37883	–0.582761	0.762766	2.55883	–0.520473	1.64154
0.0094	–0.605613	–2.37911	–0.582694	0.76248	2.5589	–0.520321	1.64216
0.0095	–0.605719	–2.37925	–0.582662	0.762341	2.55893	–0.520247	1.64246
0.0096	–0.605823	–2.37939	–0.58263	0.762205	2.55896	–0.520175	1.64276
0.0099	–0.606115	–2.37977	–0.582542	0.761825	2.55905	–0.519972	1.64359

Table 4 Real Classical Deflection Angle Calculated Values for $0.001 < \epsilon < 0.01$ where $\mu_3 = -\mu_1, \mu_4 = -\mu_2$

ϵ	α_c	θ_1	θ_2	θ_3	θ_4	μ_1	μ_2
0.0023	2.443	–2.501	–0.5537	0.6409	2.588	−0.4528	2.009
0.0024	2.441	−2.504	−0.5529	0.6377	2.589	−0.4510	2.022
0.0025	2.439	−2.507	−0.5521	0.6346	2.589	−0.4492	2.036
0.0026	2.436	−2.51	−0.5514	0.6316	2.59	−0.4474	2.049
0.0027	2.434	−2.513	−0.5506	0.6286	2.591	−0.4457	2.062
0.0028	2.432	−2.516	−0.5499	0.6256	2.592	−0.4439	2.076
0.0029	2.43	−2.519	−0.5492	0.6228	2.592	−0.4423	2.089
0.0030	2.428	−2.522	−0.5485	0.6199	2.593	−0.4406	2.103
0.0031	2.426	−2.524	−0.5478	0.6171	2.594	−0.439	2.116
0.0032	2.423	−2.527	−0.5471	0.6144	2.595	−0.4373	2.13
0.0033	2.421	−2.53	−0.5464	0.6116	2.595	−0.4357	2.143
0.0035	2.417	−2.535	−0.5451	0.6063	2.597	−0.4326	2.171
0.0036	2.416	−2.538	−0.5444	0.6037	2.597	−0.4311	2.185
0.0037	2.414	−2.54	−0.5438	0.6011	2.598	−0.4295	2.198
0.0038	2.412	−2.543	−0.5431	0.5986	2.598	−0.428	2.212
0.0039	2.41	−2.546	−0.5425	0.5961	2.599	−0.4265	2.227
0.0040	2.408	−2.548	−0.5418	0.5936	2.6	−0.4251	2.241
0.0042	2.404	−2.553	−0.5406	0.5887	2.601	−0.4221	2.269
0.0043	2.403	−2.555	−0.54	0.5863	2.602	−0.4207	2.284
0.0044	2.401	−2.558	−0.5394	0.5839	2.602	−0.4193	2.298
0.0045	2.399	−2.56	−0.5388	0.5816	2.603	−0.4179	2.313
0.0046	2.397	−2.562	−0.5382	0.5792	2.603	−0.4165	2.328
0.0047	2.396	−2.565	−0.5376	0.5769	2.604	−0.4151	2.343
0.0048	2.394	−2.567	−0.537	0.5747	2.605	−0.4137	2.358
0.0049	2.392	−2.569	−0.5364	0.5724	2.605	−0.4124	2.373
0.0050	2.391	−2.571	−0.5358	0.5702	2.606	−0.411	2.389
0.0051	2.389	−2.574	−0.5353	0.5679	2.606	−0.4097	2.404
0.0052	2.387	−2.576	−0.5347	0.5657	2.607	−0.4083	2.42
0.0053	2.386	−2.578	−0.5341	0.5635	2.607	−0.407	2.435
0.0054	2.384	−2.58	−0.5336	0.5614	2.608	−0.4057	2.451
0.0055	2.382	−2.582	−0.533	0.5592	2.609	−0.4044	2.468
0.0057	2.379	−2.587	−0.5319	0.555	2.61	−0.4018	2.5
0.0058	2.378	−2.589	−0.5314	0.5529	2.61	−0.4005	2.517
0.0059	2.376	−2.591	−0.5308	0.5508	2.611	−0.3993	2.534
0.0060	2.375	−2.593	−0.5303	0.5487	2.611	−0.398	2.55
0.0061	2.373	−2.595	−0.5297	0.5467	2.612	−0.3968	2.568
0.0062	2.372	−2.597	−0.5292	0.5447	2.612	−0.3955	2.585
0.0063	2.37	−2.599	−0.5287	0.5426	2.613	−0.3943	2.602
0.0067	2.364	−2.607	−0.5266	0.5347	2.615	−0.3894	2.675
0.0068	2.363	−2.609	−0.526	0.5327	2.616	−0.3882	2.693
0.0069	2.361	−2.611	−0.5255	0.5308	2.616	−0.387	2.712
0.0070	2.36	−2.613	−0.525	0.5289	2.617	−0.3858	2.731
0.0071	2.359	−2.615	−0.5245	0.5269	2.617	−0.3846	2.75
0.0072	2.357	−2.617	−0.524	0.525	2.618	−0.3834	2.77
0.0073	2.356	−2.618	−0.5235	0.5231	2.618	−0.3823	2.79
0.0075	2.353	−2.622	−0.5225	0.5194	2.619	−0.3799	2.83
0.0076	2.352	−2.624	−0.522	0.5175	2.62	−0.3788	2.85
0.0078	2.349	−2.628	−0.521	0.5138	2.621	−0.3765	2.892
0.0079	2.348	−2.63	−0.5205	0.512	2.621	−0.3753	2.914
0.0080	2.346	−2.6310	−0.5200	0.5102	2.622	−0.3742	2.936

$$V_3(x_B) = 2x_B^3[A(x_B) - 8\pi M^2 C_2]\,. \tag{A.9}$$

$$\begin{aligned} V_1(x_C) &= \pi/8x_C^3 + 2x_C[A(x_C) + B(x_C)/6] \\ &\quad -8\pi M^2 C_2 x_C\,, \end{aligned} \tag{A.10}$$

$$\begin{aligned} V_2(x_C) &= \frac{\pi x_C^2(1+4x_C^2)[A(x_C) - 8\pi M^2 C_2]}{2G(x_C)} \\ &\quad \Big[\frac{\pi}{4x_C^2} + 4A(x_C) + \frac{2B(x_C)}{3} \\ &\quad -16\pi M^2 C_2\Big]\,, \end{aligned} \tag{A.11}$$

$$V_3(x_C) = -\frac{x_C^3[A(x_C) - 8\pi M^2 C_2]}{2}\,, \tag{A.12}$$

where $A(x,\varepsilon)$, $B(x,\varepsilon)$, $G(x,\varepsilon)$ and C_2 are defined as

$$\begin{aligned} A[x,\varepsilon] &= \frac{1}{24x^6} - \frac{1}{4x^5} + \frac{1}{2x^4} - \frac{1}{3x^3} \\ &\quad -\frac{\epsilon}{8x^2} + \frac{\epsilon}{4x}\,, \end{aligned} \tag{A.13}$$

$$\begin{aligned} B[x,\varepsilon] &= \frac{3}{8x^6} - \frac{2}{x^5} + \frac{7}{2x^4} - \frac{2}{x^3} + \frac{x^2\epsilon^2}{8} \\ &\quad -\frac{\epsilon}{2x^2} + \frac{\epsilon}{x} - \frac{\epsilon}{2}\,, \end{aligned} \tag{A.14}$$

$$\begin{aligned} G[x,\varepsilon] &= \pi - 64\pi C_2 M^2 x^2 + 16x^2[A(x,\epsilon) \\ &\quad +\frac{1}{6}B(x,\epsilon)]\,, \end{aligned} \tag{A.15}$$

$$\begin{aligned} C_2 &= \Big[18\left(3A\left(x_B,\epsilon\right) - A\left(x_C,\epsilon\right)\right) + 5B\left(x_B,\epsilon\right) \\ &\quad -B\left(x_C,\epsilon\right)\Big]/240\pi M^2\,. \end{aligned} \tag{A.16}$$

References

Alberto, C. S., & Philip, M. 2002, Astronom. J., 123, 2312

Ansoldi, S. 2007, Apeared in the Proceedings of BH2, Dynamics and Thermodynamics of Black Holes and Naked Singularities (Milano, Italy) (arXiv:0802.0330)

Ayón-Beato, E., & García, A. 2000, Physics Letters B, 493, 149

Banados, M., Teitelboim, C., & Zanelli, J. 1992, Physical Review Letters, 69, 1849

Bardeen, J. 1968, Proc. GR5 (Tiflis, USSR)

Bender, R., Kormendy, J., Cornell, M. E., & Fisher, D. B. 2015, ApJ, 807, 56

Bower, G. A., Green, R. F., Danks, A., et al. 1998, ApJ, 492, L111

Bozza, V., de Luca, F., & Scarpetta, G. 2006, Phys. Rev. D, 74, 063001

Bozza, V. 2008, Phys. Rev. D, 78, 103005

Carlip, S. 1995, Classical and Quantum Gravity, 12, 2853

Casals, M., Fabbri, A., Martínez, C., & Zanelli, J. 2016, arXiv:1608.05366

Dey, T. K., & Sen, S. 2008, Modern Physics Letters A, 23, 953

Eiroa, E. F., Romero, G. E., & Torres, D. F. 2002, Phys. Rev. D, 66, 024010

Eiroa, E. F. 2005, Phys. Rev. D, 71, 083010

Eiroa, E. F., & Sendra, C. M. 2011, Classical and Quantum Gravity, 28, 085008

Emsellem, E. 2013, MNRAS, 433, 1862

Gaensler, B. 2012, Extreme Cosmos: A Guided Tour of the Fastest, Brightest, Hottest, Heaviest, Oldest, and Most Amazing Aspects of Our Universe

Ghaffarnejad, H., Neyad, H., & Mojahedi, M. A. 2013, Ap&SS, 346, 497

Ghisellini, G., Foschini, L., Volonteri, M., et al. 2009, MNRAS, 399, L24

Ghisellini, G., Della Ceca, R., Volonteri, M., et al. 2010, MNRAS, 405, 387

Ghisellini, G., Tagliaferri, G., Sbarrato, T., & Gehrels, N. 2015, MNRAS, 450, L34

Gyulchev, G. N., & Yazadjiev, S. S. 2008, Phys. Rev. D, 78, 083004

Hlavacek-Larrondo, J., Allen, S. W., Taylor, G. B., et al. 2013, ApJ, 777, 163

Keeton, C. R., & Petters, A. O. 2005, Phys. Rev. D, 72, 104006

Kormendy, J., & Richstone, D. 1992, ApJ, 393, 559

Kormendy, J., Bender, R., Ajhar, E. A., et al. 1996, ApJ, 473, L91

Kraniotis, G. V. 2014, General Relativity and Gravitation, 46, 1818

Lewis, G. F., Chapman, S. C., Ibata, R. A., Irwin, M. J., & Totten, E. J. 1998, ApJ, 505, L1

Liu, T., Gezari, S., Heinis, S., et al. 2015, ApJ, 803, L16

Loewenstein, M., Mushotzky, R. F., Angelini, L., Arnaud, K. A., & Quataert, E. 2001, ApJ, 555, L21

López-Cruz, O., Añorve, C., Birkinshaw, M., et al. 2014, ApJ, 795, L31

Matson, J. 2011, Brilliant, but Distant: Most Far-Flung Known Quasar Offers Glimpse into Early Universe, Scientific American, 29

McConnell, N. J., Ma, C.-P., Gebhardt, K., et al. 2011, Nature, 480, 215

McDonald, M., Bayliss, M., Benson, B. A., et al. 2012, Nature, 488, 349

Mortlock, D. J., Warren, S. J., Venemans, B. P., et al. 2011, Nature, 474, 616

Petters, A. O., Levine, H., & Wambsganss, J. 2001, Singularity Theory and Gravitational Lensing (Boston: Birkhäuser)
Romani, R. W. 2006, AJ, 132, 1959
Schneider, P., Ehlers, J., & Falco, E. E. 1992, Gravitational Lenses (Berlin: Springer-Verlag), 112
Schneider, P. 2006, in Saas-Fee Advanced Course 33: Gravitational Lensing: Strong, Weak and Micro, eds. G. Meylan, P. Jetzer, P. North, P. Schneider, C. S. Kochanek, & J. Wambsganss, 269
Sereno, M. 2008, Phys. Rev. D, 77, 043004
Sereno, M., & de Luca, F. 2006, Phys. Rev. D, 74, 123009
Shen, J., & Gebhardt, K. 2010, ApJ, 711, 484
Trakhtenbrot, B., Urry, C. M., Civano, F., et al. 2015, Science, 349, 168
Valtonen, M. J., Ciprini, S., & Lehto, H. J. 2012, MNRAS, 427, 77
Virbhadra, K. S., Narasimha, D., & Chitre, S. M. 1998, A&A, 337, 1
Walker, S. A., Fabian, A. C., Russell, H. R., & Sanders, J. S. 2014, MNRAS, 442, 2809
Walsh, J. L., Barth, A. J., Ho, L. C., & Sarzi, M. 2013, ApJ, 770, 86
Weinberg, S. 1972, Gravitation and Cosmology: Principles and Applications of the General Theory of Relativity (Wiley-VCH), 688
Wu, X.-B., Wang, F., Fan, X., et al. 2015, Nature, 518, 512
Zuo, W., Wu, X.-B., Fan, X., et al. 2015, ApJ, 799, 189